Applied Physics A (2021) 127:612
https://doi.org/10.1007/s00339-021-04724-1

Applied Physics A
Materials Science & Processing

Recent developments in recalcitrant organic pollutants degradation using immobilized photocatalysts

Kareem Fouad[1,2] · Mohamed Bassyouni[3,4] · Mohamed Gar Alalm[5,6] · Mamdouh Y. Saleh[1]

Received: 8 May 2021 / Accepted: 24 June 2021 / Published online: 20 July 2021

Abstract

Immobilization or coating of photocatalysts on supporting media can open a new avenue for industrial application of photocatalysis in wastewater treatment. Herein, we present a critical review of the recent advances in loading photocatalysts on different materials to degrade such bio-recalcitrant organics as pharmaceuticals, pesticides, surfactants, and dyes, which helps in the sustainable use of polluted water after treatment. Many of the recently developed photocatalysts have proven high stability for long periods under illumination. Consequently, employing the catalysts in retained forms provided a viable solution for reuse. Supports may be movable; these include zeolites, polymers, quartz sand, 3-D graphene or fixed, such as glass plates, aluminum plates, and stainless steel plates. Photocatalytic reactors could be an ideal solution for continuous operating treatment, especially in a large-scale operation. In this review, the use of suspended and immobilized systems are compared in the degradation of bio-recalcitrant organic pollutants. Despite the limited research used in the immobilized systems, this proved very successful. This technique has overcome many of the other suspended systems' problems, affording economical solutions such as the possibility of repeated reuse of the catalyst, reduced risk of the catalyst escaping with treated water, and the possibility of application on an industrial scale.

Graphical abstract

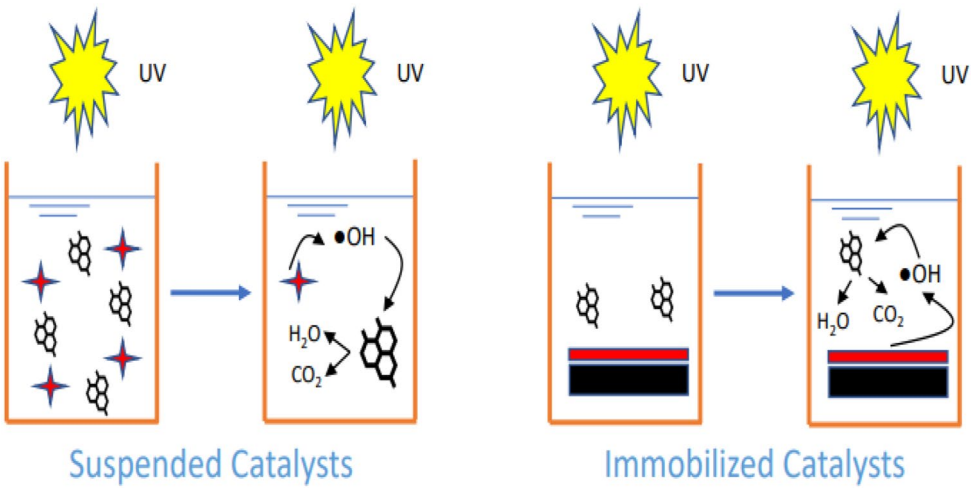

Keywords Wastewater · Recalcitrant organic pollutants · Photocatalysts · Supporting materials · Immobilization · Catalyst supports · Reactors

✉ Mohamed Bassyouni
mbassyouni@zewailcity.edu.eg

Extended author information available on the last page of the article

Abbreviations

ROPs	Recalcitrant organic pollutants
WWTPs	Wastewater treatment plants
AOPs	Advanced oxidation processes

NPs	Nanoparticles
PCO	Photocatalytic oxidation
CB	Conduction band
NSAIDs	Non-steroidal anti-inflammatory drugs
AEDs	Antiepileptic drugs
b-blockers	Beta-blockers
MCP	Monocrotophos
AP	Antipyrine
MMT	Montmorillonite
DCF	Diclofenac
Goe	Goethite
Mf	Maleate ferroxane
PAN	Polyacrylonitrile
MET	Metronidazole
MWCNTs	Multi-wall carbon nanotubes
SMX	Sulfamethoxazole
PFOSAs	Perfluorosulfonamides
PFSAs	Perfluorosulfonates
PFOS	Perfluorooctane sulfonate
PFCAs	Perfluorocarboxylic acids
PFOA	Perfluorooctanoic acid
BPA	Bisphenol A (2,2-bis(4-hydroxyphenyl) propane)
PVDF	Polyvinylidene fluoride
CDT	Carbon-doped TiO_2
GAC	Granular activated carbon
WPC	White Portland cement
MB	Methylene blue
MG	Malachite green oxalate
MO	Methyl orange
DMP	Dimethylphenol
AC	Activated carbon
OMC	Mesoporous Carbon
SMFs	Sintered Metal Fibers
TCE	Trichloroethene
TSA	Tungstosilicic acid
CIP	Ciprofloxacin
CEX	Cephalexin
PhACs	Pharmaceuticals
3D GBMs	Three-dimensional graphene-based materials
CVD	Chemical vapor deposition
SM	Steel mesh
SEM	Scanning electron microscope
XRD	X-ray diffraction
UV–Vis	Ultraviolet-visible spectroscopy
MZTC	Modified zeolite/TiO_2 composite
RGOT	Reduced graphene oxide/TiO_2
HS	Humic substances
DCP	Dichlorophenol
MOCVD	Metal-Organic Chemical Vapor Deposition
IMI	Imidacloprid
GFC	Glass fiber cloth
TEOA	Triethanolamine
ISO	Isopropanol
AO	Ammonium oxalate
BQ	Benzoquinone
EDTA	Edetic acid
EDTA-2Na	Edetate disodium
KI	Potassium iodide
COS	Carbon oxidation state
AOS	Average oxidation state; SMZ, Sulfamethazine

1 Introduction

Over recent decades, pollution has become common [1]. With industrial progress and extensive use of complex chemicals, many such substances are present in our water sources. Since these substances are complicated to degrade, they represent a real threat to our ecosystem. Significantly, their presence has increased over time, representing a dangerous challenge for future generations. Therefore, we must attempt to understand the nature of these materials and try to find appropriate solutions. Recalcitrant organic pollutants (ROPs) refers to organics like agrochemicals, phenols, dyes, surfactants, pesticides, and pharmaceuticals that can disperse the environment and damage animals and human life [2–6]. Recalcitrant organic pollutants successful elimination from aquatic ecosystems is crucial not only for the purification of water but also for preserving social and environmental health [7–9]. Recalcitrant organic pollutants inadequate degradation by wastewater treatment plants (WWTPs) occurred because WWTPs were never intended to treat these pollutants; in some situations, removal of such contaminants was below 10% [10–14].

Advanced oxidation processes (AOPs) have virtually eliminated ROPs from the solution [15–19]. Semiconductor photocatalysis materials are a critical AOPs technique for the remediation of contaminated water such as TiO_2 [20]. Advanced oxidation processes technology is dependent on developing highly reactive in situ hydroxyl radicals (•OH), which interact with supreme organics in a non-selective manner and can degrade even highly recalcitrant compounds [21–26]. In this process, •OH radicals initiate a series of oxidation reactions that lead to H_2O and CO_2 [27–30]. In contrast, employing catalysts nanoparticles (NPs) for the degradation of these contaminants is quite difficult on the industrial scale [31]. The separation and recovery of the costly active catalyst is a basic problem related to their limited use for industrial and synthetic purposes [32, 33]. Moreover, the extensive use of nanomaterials entering the ecological environment leads to destruction of algae growth. Therefore, the aquatic ecosystem's balance can be damaged [34, 35]. For example, NPs of TiO_2 have been classed as

"harmful" for species like bacteria, yeast, algae, nematodes, crustaceans, and fish, at a concentration between 10 and 100 $mg.ml^{-1}$ [36]. Immobilization of semiconductor photocatalysis on supports is an ideal solution to prevent leakage of these nanoparticles after the treatment. Moreover, the reusability of the photocatalysts is hindered by the tedious and costly collecting of particles, which may require ultrafiltration. On the other hand, the photocatalyst body is not consumed during the photocatalytic reaction, which allows effective reuse until the catalyst surface is blocked by the accumulation of adsorbed organic molecules. Considering the high cost of most photocatalysts, reactors that employ the catalysts in retained form can be the shortest avenue for the application of photocatalysis on larger scales [37, 38].

There are two categories of AOPs (heterogeneous and homogenous catalysis) [39]. A catalyst is classified as homogenous if it exists in the same phase as the regents. Ozone and the Fenton method (Fe^{+} and Fe^{+}/H_2O_2) are the most widely applied catalysts [40]. In contrast, if a catalyst exists in a phase other than the reaction mixture, it is classified as heterogeneous. Separating heterogeneous catalysts is simple from the interactive media, and could be reused repeatedly [41].

Heterogeneous photocatalysis is a promising technology that is a practical, environmentally friendly, and economical technique for the degradation of organic impurities [42]. Electrochemical oxidation and reduction reactions are the immediate reactions in semiconductor photocatalysis, which involves transferring holes and electrons from the photoexcited semiconductor [43]. Several metal oxides are used as heterogeneous photocatalysts, including Fe_2O_3, TiO_2, $NaTaO_3$, $SrTiO_3$, V_2O_5, NB_2O_5, WO_3, ZnO [44–50]. Sulfides including CdS, Co_3S_4, MoS_2, ZnS, In_2S_3 [27, 51], and halides (AgCl, BiOI, AgBr) [52, 53] may also be deployed. Transition metal sulfide nanoparticles have unique size-dependent optical, electrical, electronic, and magnetic properties that distinguish them from bulk materials, as well as uses in catalysts [54, 55]. Because of their light absorption properties, charge-transfer characteristics, excited-state endurance, and electronic structures, oxide-based semiconductors are generally good choices for photocatalytic applications. Electronic band gaps in semiconductor materials are commonly low. Although the cocatalysts drive surface redox processes through kinetic control, they operate as a charge-releasing and light-absorbing substance [56]. M. Junaid et al. [57] studied Fe-doped CdS nanoparticles for the degradation of MB dye. The results showed a reduction in cost and complete removal of dyes. Desirable heterogeneous photocatalysts for practical environmental requirements should be safe, cost-effective, stable, efficient, and visible light-responsive, as shown in Fig. 1 [58]. The expression "photocatalytic degradation" commonly describes full photocatalytic oxidation or photo-mineralization, especially to H_2O, NO_3^{-}, CO_2, PO_4^{3-} [22]. In this study, the conventional use of photocatalysts in suspended form is reviewed. Despite this high-efficiency method, application in water treatment plants or at industrial scale is inappropriate or limited due to the difficulty of catalyst collection with filtration and hazard of catalyst if it escaped with treated water. On the other hand, immobilized catalysts are used as a practical solution to overcome previous problems, and the application in the degradation of recalcitrant organic pollutants may be possible, as may the possible use of immobilized catalysts in wastewater treatment plants in several cycles with high efficiency.

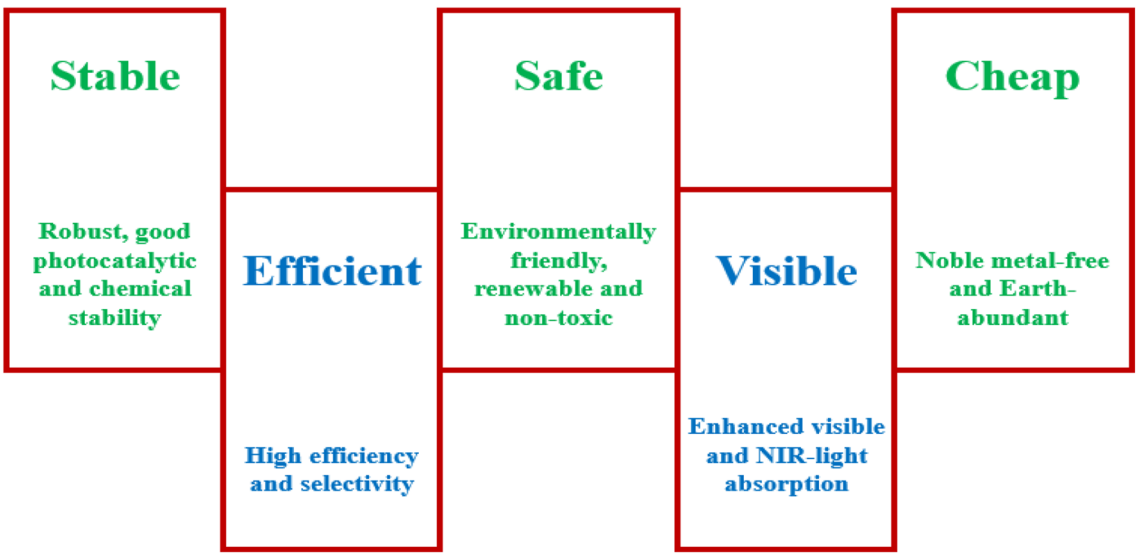

Fig. 1 Practical environmental requirements for homogeneous photocatalysts

1.1 Heterogeneous photocatalysis process methodology

The heterogeneous photocatalysis process includes a sequence of reductive and oxidative reactions. The highest-unoccupied and lowest-occupied energy bands in a semiconductor are separated by a band gap, indicated by E_{bg}. As light energy (photons) bearing photon energy equal to or higher than the semiconductor's E_{bg} is illuminated on its surface, the electrons from the valence bands are photoexcited and transferred in femtoseconds to the conduction band (CB) [59]. This leaves behind an unfilled valence band, called a hole (h^+), forming an electron–hole pair. If these holes and electrons are trapped on the surface of the semiconductor, and their combination is avoided, a series of reactions is initiated, as follows [60, 61]:

$$\text{Photoexcitation}: TiO_2 + h\upsilon \rightarrow e^-_{CB} + h^+_{VB} \quad (1)$$

$$\text{Entrapment of free electrons}: e^-_{CB} \rightarrow e^-_{TR} \quad (2)$$

$$\text{Entrapment of holes}: h^-_{CB} \rightarrow h^+_{TR} \quad (3)$$

$$\text{Charge carrier recombination}: e^-_{TR} + \lambda^+_{VB} \rightarrow e^-_{CB} + \text{heat} \quad (4)$$

$$\text{Photoexcited electron scavenging}: (O_2)_{ads} + e^-_{CB} \rightarrow O_2^{\cdot -} \quad (5)$$

$$\text{Oxidation of hydrolysis}: OH^- + h^+_{VB} \rightarrow {}^{\cdot}OH \quad (6)$$

$$\text{Photodegradation by } OH^- \text{ radicals}: R - H + {}^{\cdot}OH \rightarrow R^{/\cdot} + H_2O^{\cdot} \quad (7)$$

A successful photocatalytic reaction occurs by absorbing photons to generate e − /h + pairs. The incident light energy must be larger than the band gap of the semiconductor [62]. When photons are irradiated on a semiconductor with an energy equal to or greater than the energy of its band gap (3.2 eV in TiO_2 and ZnO, respectively), the photons are absorbed, resulting in the formation of electron–hole pairs. These electrons and holes can recombine or separate. They move to the surface, taking part in a variety of activities. Eventually, redox reactions lead to the production of reactive oxygen species (ROS), such as OH radicals, reactive oxygen species (ROS) as well as H_2O_2. These transient ROS have the ability to start and stop a variety of responses. Pollutants are completely mineralized and rendered harmless CO_2 products.

Many of the commonly used semiconductors have wide band gaps and can thus only be excited under irradiation of UV light. Because Fig. 2 explains photocatalytic semiconductors' mechanism of oxidation by reactive oxidant species [63]. The radicals of $OH^{\bullet}$ produced in Eq. (2.6) reduce organic contaminants into intermediate products, which continue to decompose until release of CO_2 and H_2O as by-products (as in Eq. (7)). The inclusive response is outlined in the procedures below [64]:

- Organic impurities or mass transfer of bacteria from the bulk liquid phase to the face of the photocatalyst.
- Pollutant adsorption to photocatalyst surface activated by the photon.
- H_2O_2 and $^{\bullet}OH$ radicals production followed by pollutant chemical degradation.
- Photocatalyst surface desorption of the final products or intermediate.

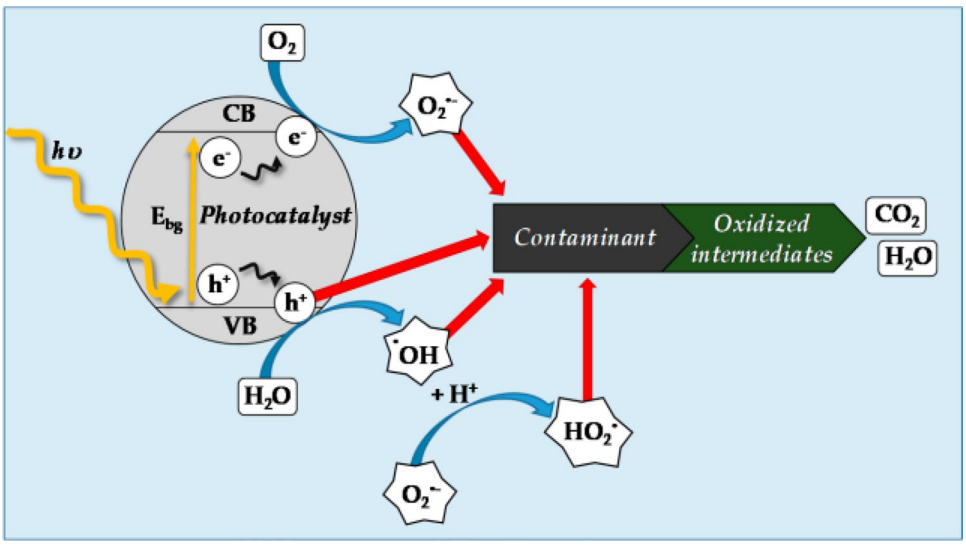

Fig. 2 Schematic representation of photocatalytic semiconductors mechanism for contaminates oxidation by reactive oxidant species [63]

- Final component or intermediate mass transfer into the liquid bulk phase [64].

2 Recalcitrant organic pollutants

Municipal and industrial wastewaters including recalcitrant organic compounds are among the major sources of surface water pollution discharge from urban wastewater treatment plants [65]. Because they contain an aromatic ring, the majority of such compounds are resistant to conventional treatments like coagulation, adsorption, ion exchange, biological oxidation, and chemical oxidation [2, 21, 66]. Recalcitrant contaminants, like pharmaceuticals, aromatics, agrochemicals, phenolic components, surfactants, dyes, etc., are difficult to degrade under the natural state. Some of their harmful effects include physiological damage, including reproductive failure, increased risk of cancer in marine and terrestrial organisms, and potential development of antibiotic-resistant bacteria. Recalcitrant organic classes are shown in Fig. 3; the toxic consequences of such recalcitrant chemical mixtures, and the environmental effects of many emerging contaminants are still unknown [67, 68]. The mechanism of recalcitrant organic pollutant degradation using sensitized TiO_2 photocatalysis in the irradiation of visible light has been reported by Han et al. [69]. Equations (8)-(14) outline the mechanism's main steps under visible irradiation [69].

$$\mathrm{ROPs} + h\upsilon \rightarrow \mathrm{ROPs}^{*} \tag{8}$$

$$\mathrm{ROPs}^{*} + \mathrm{TiO_2} \rightarrow \mathrm{ROPs}^{\cdot +} + \mathrm{TiO_2}(e^{-}_{CB}) \tag{9}$$

$$\mathrm{TiO_2}(e^{-}_{CB}) + \mathrm{O_2} \rightarrow \mathrm{TiO_2} + \mathrm{O_2^{\cdot -}} \tag{10}$$

$$\mathrm{O_2^{\cdot -}} + \mathrm{TiO_2}(e^{-}_{CB}) + 2\mathrm{H}^{+} \rightarrow \mathrm{H_2O_2} + \mathrm{TiO_2} \tag{11}$$

$$2\mathrm{O_2^{\cdot -}} + 2\mathrm{H}^{+} \rightarrow \mathrm{O_2} + \mathrm{H_2O_2} \tag{12}$$

$$\mathrm{H_2O_2} + \mathrm{TiO_2}(e^{-}_{CB}) \rightarrow \cdot\mathrm{OH} + \mathrm{OH}^{-} + \mathrm{TiO_2} \tag{13}$$

$$\mathrm{ROPs}^{\cdot +} + (\mathrm{O_2^{\cdot -}} \text{ or } {}^{\cdot}\mathrm{OH}) \rightarrow \text{the degradation products} \tag{14}$$

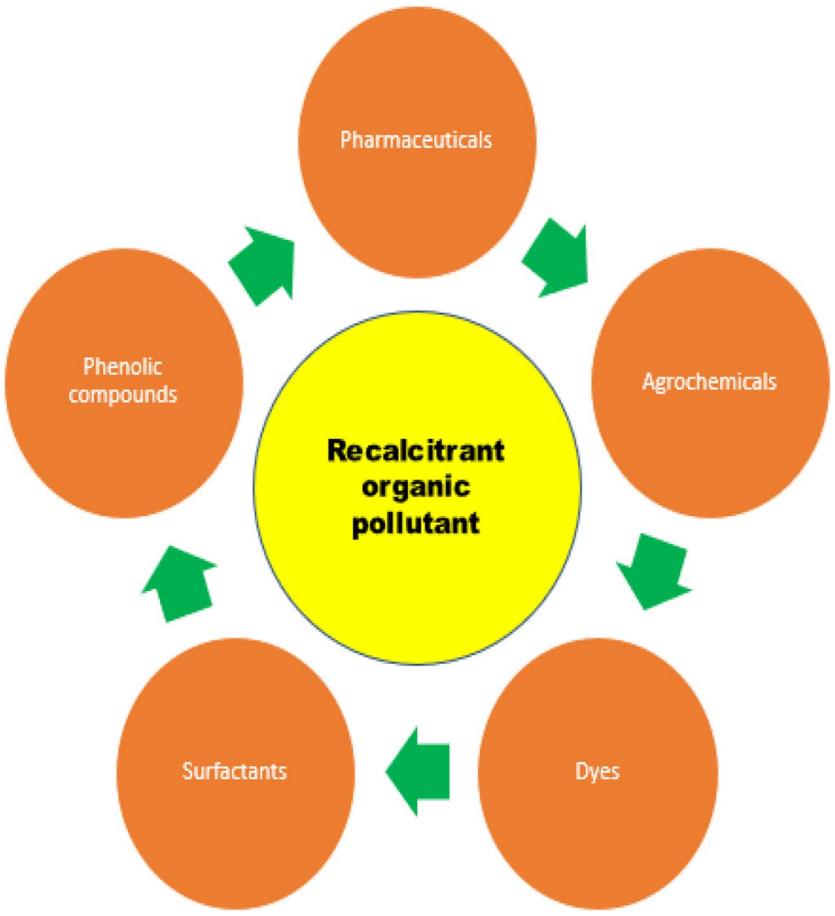

Fig. 3 Classification of recalcitrant organic pollutants

2.1 Pharmaceuticals

Recently, because of a widespread uses in many fields such as in the text (medicine, livestock, farming and aquaculture, pharmaceuticals) have been found in many sources of water such as wastewater effluent [70–75], surface water [76–79], groundwater [80, 81], and even in drinking water [82, 83]. Most of those pharmaceutical drugs consumed and prescribed by livestock and humans are later excreted and discharged in WWTPs [84–88]. Pharmaceuticals in the ecosystem can damage the microbial community's function and behaviors in several ways [89]. Antibiotic resistance in the human body and antibiotic resistance of microorganisms have been increased and aroused by the abuse and misuse of antibiotics [90]. Because of its properties, several countries count effluent from hospitals as industrial wastewater, and it is submitted to pre-treatment before being discharged into the urban sewage network [91]. Classical biological treatment is not adequate for removing pharmaceuticals due to their recalcitrant performance [92–94].

Concerning environmental series of pharmaceuticals involves non-steroidal anti-inflammatory drugs (NSAIDs), antibiotics, antiepileptic drugs (AEDs), beta-blockers (b-blockers), antidepressants, blood lipid-lowering agents, antihistamines, hormones [71, 95, 96]. Although these substances are difficult to degrade, various successful attempts to remove pharmaceutical drugs using immobilized photocatalysts have been detected. Table 1 summarizes successfully degraded pharmaceutical drugs using immobilized photocatalysts.

2.2 Pesticides

Among different categories of ROPs, pesticides are the most commonly used worldwide, applied in regions including 6.5–60 kg.ha^{-1}, which adds 2.5 million tons per year [97]. Pesticide usage in agricultural practices is essential, as ensuring the quality of the harvest and food protection. Releasing these elements to the ecological system, including freshwater organisms, may threaten them by exposure to pesticides, which are commonly recognized to contain life-threatening chemicals [98–102].

Several researchers have proposed using biological, chemical, and physical approaches to treat wastewater containing pesticides. These methods were unfavorable due to their expensive cost and insignificant removal efficiency [103, 104]. However, AOPs techniques demonstrated a significant removal efficiency toward various pesticides [105, 106]. Table 2 illustrates successfully degraded pesticides using immobilized photocatalysis. Pesticides' main categories are insecticides, fungicides, herbicides, bactericides, etc. [107]. Moreover, pesticides are classified according to:

- Chemical class (organophosphates, organochlorines, etc.).
- Function requirement (public health, agriculture, domestic).
- Purpose (Target organism: herbicide, insecticide, fungicide, etc.) [108].

2.3 Surfactants

Surfactants are organic molecules that include hydrophilic classes (their heads) and hydrophobic classes (their tails). They are categorized according to their ionic properties in water as cationic (positive charge), nonionic (no charge), either anionic (negative charge), or amphoteric (negative/positive charge based on pH) [109]. Surfactants are utilized to reduce the tension on the surface between two liquids or between a solid and a liquid, making them appropriate as detergents, emulsifiers, foaming agents, wetting agents, and dispersants [110]. They are extensively used in detergents, pesticides, cosmetics, shampoos, and other consumer products. Some surfactant compounds are not rapidly biodegradable, so high residuals are found in the treated effluents [111, 112]. After using these surfactants, the residue and the degradation outcomes are released into marine ecosystems and are included in different environmental sections such as surface waters [113]. Surfactants consist of hydrophilic and hydrophobic moieties. Despite these compounds' seriousness, they need to be degraded by applying immobilized photocatalysts as there is minimal research in this field.

Noorimotlagh et al. [114] reported carbon-doped TiO_2 (CDT) immobilized on a granular surface of activated carbon (GAC). It was used for commercial surfactant of nonylphenol (NP) photocatalytic degradation. TiO_2 nanoparticles were in various ratios of rutile (R) and anatase (A) parts. Photocatalyst CDT/GAC at R (46.94)/A (53.06) revealed significant degradation efficiency. Removal of TOC and COD was 89% and 99%, respectively, decreasing to 80% of NP within 60 min. Li et al. [115] studied PFOA degradation using Pb-$BiFeO_3$ immobilized on rGO sheets as a heterogeneous catalyst in a microwave-enhanced Fenton-like process. For PFOA degradation, a greater catalytic efficiency was shown by the composite of Pb-BFO/rGO for H_2O_2 activation with the removal of 90.0% within 5.0 min. Gomez-Ruiz et al. [116] demonstrated the degradation of PFOA using TiO_2-rGO catalyst. A TiO_2-based composite catalyst of 95% and reduced graphene oxide 5% was synthesized by a simple hydrothermal process. After 12 h of UV–vis illumination, PFOA's degradation efficiency reached 93 ± 7% by using a 0.1 g L^{-1} of TiO_2-rGO composite at an initial PFOA concentration 0.24 mmol.L^{-1}. The illumination source was a medium-pressure mercury lamp, and a significant increase

Table 1 Pharmaceutical drugs successfully degraded by immobilized photocatalysts

Drugs, Series	Catalyst	Support	Experimental conditions	Main outcomes	Reference
Ibuprofen, (NSAIDs)	TiO_2-rGO	Optical Fibers	Operating conditions: halogen lamp; 150 W, a pack of 30 pieces photocatalyst-coated SOFs fiber, pharmaceuticals (Ibuprofen) initial concentration 5 mg L^{-1}, pH 6, T 23◦C	Removal of 57% for ibuprofen after 6-h visible light irradiation	[218]
Naproxen, (NSAIDs)	ZnO	Montmorillonite	Operating conditions: naproxen initial concentration varied from 5 to 20 mg L^{-1}, pH ranges 4.5–11, the maximum wavelength of 230 nm, the irradiation time of 120 min, the dosage of ZnO/MMT from 0.25 to 1.25 g L^{-1}	Maximum removal was at ZnO/MMT dosage 1.25 g L^{-1}, naproxen initial concentration 5 mg L^{-1}, pH 4.5	[219]
Salicylic acid, (NSAIDs)	P25-TiO_2/Tetraethylorthosilicate	Glazed ceramic	Operating conditions: visible light, the intensity of incubator was 10,000 ± 1000 × with uniform humidity and ventilation, temperature 25 °C, atmospheric pressure, 50 mL beakers, glazed ceramic tiles 25 mm × 25 mm × 5 mm, Salicylic acid concentration is 5 mg L^{-1}	Maximum degradation was attained and kept constant up to 10 h, under optimum conditions diclofenac, naproxen, ibuprofen, and salicylic acid degradation are 65%, 94%, 85%, and 76%, respectively	[220]
Diclofenac, (NSAIDs)	TiO_2	Zeolite	Operating conditions: DCF initial concentration 0.1 mM, water-jacketed with (T = 25.0 ± 0.2 °C and V = 0.09 L) batch photoreactor, Xe lamp of 450 W, the intensity of light 124.78 ± 0.11 mW.cm^{-2}, time of irradiation 0, 15, 30, 45, and 60 min	DCF removal 78.6% predicted by RSM model M1, pH 4, initial concentration of H_2O_2 = 3.86 mM, FeZ percentage 25.4 wt% within the composite	[221]
Antipyrine (AP), (NSAIDs)	TiO_2	Glass disk	Operating conditions: contaminated solution 750 mL, 20 W pressure mercury UV lamp, H_2O_2 (0–2000) mg L^{-1}, pH (4–8), and Flow (0–25) mL min^{-1}	100% degradation of AP after 120 min. at optimum conditions: $[AP]_0$ = 50 mg L^{-1}, $[H_2O_2]_0$ = 1500 mg L^{-1}, pH 4, Flow = 25 mL s^{-1}, Speed = 500 rpm	[222]
Tetracycline, antibiotics	TiO_2	MWCNTs	Operating conditions: time for irradiation between 0:120 min, MWCNTs/TiO_2 was between 0.5:10, dosage of nanocomposite MWCNTs/TiO_2 ranged from 0.1:0.4 g L^{-1}, the initial pH ranged from 3:11, and initial concentration of tetracycline was between 0.5:30 mg L^{-1}	100% tetracycline was removed after 100 min	[223]
Ciprofloxacin, antibiotics	TiO_2	Carbon nanosheets	Operating conditions: CIP initial concentration varied from 5 to 40 mg L^{-1}, immobilized catalyst initial concentration 500 mg L^{-1},	Selectivity coefficient was 3.2 for photocatalysis, and 7.2 for adsorption, respectively	[224]

Table 1 (continued)

Drugs, Series	Catalyst	Support	Experimental conditions	Main outcomes	Reference
Ciprofloxacin, antibiotics	TiO_2	Glass plate	Operating conditions: flow rate 1 mL s^{-1}, glass plates 3 × 20 cm, antibiotic initial concentration varied from 3 to 9 mg L^{-1}), pH ranged from 3 to 11, and time ranges (15, 30, 45, 60, 75, 90 and 105 min)	92.81% degradation efficiency at optimum conditions time of 105 min, pH 5, ciprofloxacin initial concentration mg L^{-1}	[225]
Ciprofloxacin, antibiotics	ZnO	Stones	Operating conditions: pH varied from 3 to 11, ciprofloxacin initial concentration ranged from 5 to 20 mg L^{-1}, reaction time from 5 to 30 min, catalyst dosage range 1 to 3 g L^{-1}, a flow rate of 4 $Lmin^{-1}$, and three stones which dimensions are 3 cm in width by 20 cm in length for catalyst immobilization	96% removal efficiency of ciprofloxacin, time of reaction 30 min of reaction time at pH 7, initial concentration of ciprofloxacin 10 mg L^{-1}, and 3 g L^{-1} is the dosage of photocatalyst	[226]
Trimethoprim, antibiotics	S-TiO_2 and Ru/WO_3/ZrO_2	Aluminum plates	Operating conditions: aluminum plates dimensions in thickness and diameter are 2 mm, and 65 mm, aluminum grade is 3003, 1 g of S-TiO_2 or Ru/WO_3/ZrO_2 was uniformly distributed, 250-mL Pyrex beaker photocatalytic reactor filled trimethoprim solution of 100 mL, 400-W metal halide lamp, illumination time was from zero to 240 min	98.2% and 100% was the degradation efficiency of trimethoprim at catalyst dosage of 0.5 g L^{-1}, time of irradiation 240 min, and pH of 7.0 using suspended S-TiO2, and Ru/WO_3/ZrO_2, respectively, the degradation efficiency after five cycles were 88.6%, 86%, 84%, 78% and 75.9% in case of S-TiO_2, and 98%, 96.9%, 96.8%, 93.2% and 83.4% using Ru/WO_3/ZrO_2	[227]
Amoxicillin, antibiotics	Fe-based nanoparticles (goethite (Goe) and maleate ferroxane (Mf))	Polyacrylonitrile (PAN)	Operating conditions: filtration cell volume of 200 mL, filtration area of membrane 12.56 cm^2, each membrane pressurized firstly to 0.6 MPa up to 30 min, initial concentration of H_2O_2 460 mg L^{-1}, AMX initial concentration 105 mg L^{-1}, pH ranged from 6.5–7	86.3% and 92.3% was the AMX removal using P/G-FT, and P/M-FT, respectively, in comparison with those without Fenton reaction 83.1%, and 84% for P/G and P/M, respectively, P/G and P/M membranes showed higher performance in the removal of AMX and permeated flux than pristine PAN membranes (71% in the absence of H_2O_2), AMX was mineralized to 85.4, and 83.5% for P/M-FT and P/G-FT, respectively, in TOC analysis	[228]

Table 1 (continued)

Drugs, Series	Catalyst	Support	Experimental conditions	Main outcomes	Reference
Metronidazole, antibiotics	ZnO	Montmorillonite	Operating conditions: cylindrical quartz tube batch with a total volume of 900 mL, UV-A illumination 8 W, pH ranged from 2 to 10, MET initial concentration was ranged from 25 to 50 mg L^{-1}, Time 30 min	The degradation efficiency raised with pH increasing up to 10, the dosage of ZnO/MMT nanocomposite 50 mg L^{-1}	[229]
Cephalexin, antibiotics	TiO_2	Clay beads with waste fly ash/ foundry sand	Operating conditions: seven UV tubes 36 W, a borosilicate glass bowl of 100 mL (5 cm height and 17 cm diameter) UV intensity was 23 ± 2 W.m^{-2}, solution of 50 mL, rate of flow for inlet air 3.5 L.min^{-1}	89% was the maximum degradation efficiency of CEX after 4 h of irradiation, H_2O_2 did not significantly contribute to the photocatalytic procedure, enhancement in the degradation noticed in acidic pH, with smaller diameter beads (10 mm) the degradation raised significantly	[230]
Sulfamethoxazole (SMX), antibiotics	TiO_2	Crushed borosilicate glass	Operating conditions: SMX initial concentration was 20 mg L^{-1}, an internal diameter of 0.05 m, 0.5 m tall, 1 m of path length for a spiral borosilicate glass column, size of crushed glass (300 or 600 µm), mercury vapor lamps 250 W, (H_2O_2) initial concentration was 266 mg L^{-1}, T 30 °C, and reaction times ranged from 15 to 300 min	92% was the degradation efficiency after 300 min. Catalyst leaching was approximately 80% after repetitive cycles	[231]
Acebutolol/ propranolol, b-blockers	TiO_2/Silica	Glass slides	Operating conditions: The photocatalytic cell was a DURAN tube of glass (inner diameter 40 mm, and 250 mm length), three low-pressure mercury lamps (CLEO 20 W. T was constant at 35 ºC; b-blocker initial concentration was 25 mg L^{-1}; TiO_2 initial concentration 0.17 g L^{-1}	92% and 75% was the degradation efficiency for acebutolol and propranolol after irradiation time of 240 min	[232]
Estrone (E1)/ 17-estradiol (E2)/ 17-ethinylestradiol (EE2/ Estriol (E3), hormones	TiO_2	Porous titanium sheets	Operating conditions: 500 mL batch reactors beakers wrapped with aluminum foil, pH 4–11, six-cm collimated UV-LED beam (θbeam = 4 cm; at λ = 365 nm), average irradiance estimated at 10.5 cm is 0.390 mW.cm^{-2}., estrogen concentration 4 µg L^{-1}	Lower pH conditions (pH 4) favored, removal to below the D.L after 120 min,	[233]

Table 2 Pesticides successfully degraded using immobilized photocatalysis

Pesticide	Catalyst	Support	Experimental conditions	Main outcomes	Reference
Monocrotophos (MCP)	TiO_2	Local clay beads	Operating conditions: Two-liter of MCP initial concentration was 25 mg L^{-1}, temperature (25 ± 1 °C), natural MCP pH (pH 5), the interval time interval varied from 1 h up to 7 h	78.57% was the obtained degradation efficiency at optimum conditions as 25 mg L^{-1} initial concentration of MCP, pH 5, and 600 beads were used, the immobilized TiO_2 reusability over clay beads was performed for 30 repetitive cycles without catalyst reactivation. The COD of the MCP after degradation was 73.75%	[234]
Diazinon	MgO	Concrete	Operating conditions: plexiglass reactor of 700 mL volume, Five UV lamps, 3.43 mL s^{-1} was the flow rate, pH ranged from 5 to 9, initial concentration of diazinon 5–20 mg L^{-1}, Time 30:90 min	99.46% was the maximum revealed removal under the optimum conditions; pH 7, initial concentration of diazinon 5 mg L^{-1}, and illumination time of 120 min, energy consumption was at a minimum at; pH 7, initial concentration of diazinon 5 mg L^{-1}, and illumination time of 30 min	[235]
Diazinon	WO_3 doped ZnO	Glass substrate	Operating conditions: Plexiglas reactor (500 mL), the surface area of nanoparticles 200 cm^2, pH ranged from 3 to 11, initial light intensity ranged from 6 to 30 Watts, number of nanoparticles per unit area of the glass ranged from 2 to 10 mg cm^{-2}, initial diazinon concentration ranged from 10 to 200 mg L^{-1}, and illumination time from 20 to 180 min	99% was the maximum degradation for diazinon obtained using neutral pH, catalyst per area of glass 10 mg cm^{-2}, 2% WO_3 doped ZnO, initial concentration of 10 mg L^{-1} for diazinon, illumination time of 180 min	[236]
Monocrotophos (MCP)	TiO_2	Polymeric beads	Operating conditions: MCB initial concentration ranged from 1 to 15 mg L^{-1}, initial pH ranged from 3.5 to 10.5, and catalyst loading ranged from 2 to 6 g L^{-1}	80% was the degradation efficiency of MCP at the optimum conditions as initial concentration of MCP 1 mg L^{-1}, 4 g L^{-1} for catalyst load, and pH 7	[237]
Pyrimethanil	TiO_2	β-SiC foams	Operating conditions: initial concentration of pyrimethanil varied from 10 to 30 mg L^{-1}, flow rate ranged from 26 to 78 mL min^{-1}, reaction time ranged from 4 to 12 min	Removal efficiency 88% after 4 h	[238]
Carbendazim	TiO_2 and Fe-doped TiO_2	clay beads	Operating conditions: CBZ initial concentration 8 kg m^{-3}, pH 6.3,	77 ± 3.85% averages were the maximum degradation efficiency for carbendazim at optimum conditions, the diameter of CL beads 12.42 mm, COD reduction was 88 ± 4.4% and 72 ± 3.6% under sunlight and UV conditions, respectively	[239]
Parathion	Pd-Au nanoparticles	Amberlyst® resin	Operating conditions: 0.01 g Resin–Au–Pd, 4 mL parathion with initial concentration 10 ppm, visible light irradiation using 120 W LED light (400–700 nm), or 210 min	Optimum conditions were a catalyst amount of 100 mg, neutral pH, parathion initial concentration 10 ppm. The activity of photocatalyst is sustainable even after the six repetitive cycles	[240]

in degradation efficiency was noted compared to TiO_2 photocatalysis 24 ± 11% PFOA removal. The degradation mechanism and efficiency are shown in Fig. 4.

2.4 Dyes

Dyes are colored and appropriate for coloring leather, textiles, fibers, wool, and paper [117–120]. At present, about 100,000 various kinds of dyes are utilized by the textile industries. During the dying process, up to 20 percent of the overall global dyes production is lost and discharged in the textile discharges [39, 121–123]. Such discharge into the ecosystem of colored wastewater causes severe environmental issues and affects human health [124–126]. They are highly tinctorial and visible in polluted water even at low concentrations, and their synthetic structure and aromatic nature make them stable and hardly biodegradable [62, 127]. Dyes are classified based on chromophore structure into solvent dyes, reactive dyes, direct dyes, basic dyes, and vat dyes [128], as shown in Fig. 5. Only 47% of synthetic dyes

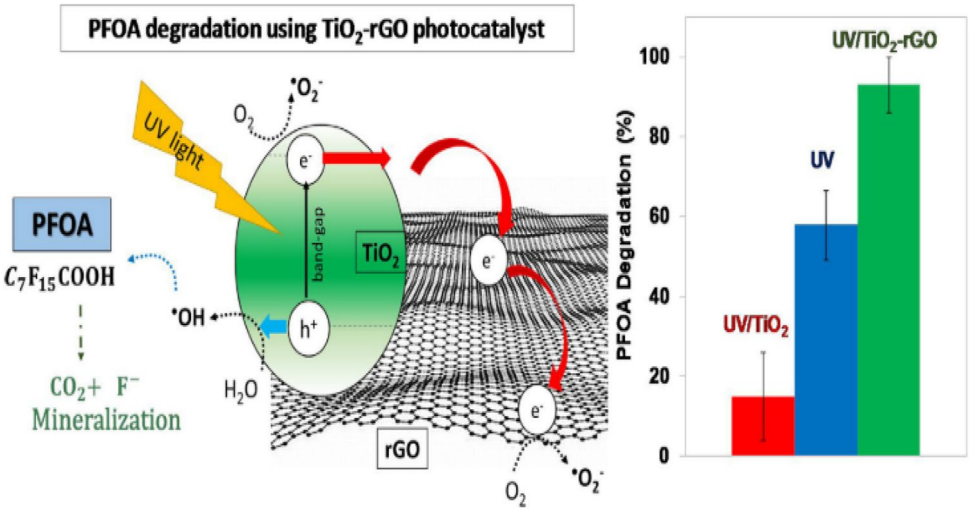

Fig. 4 Degradation mechanism for PFOA using TiO_2/rGO composite, and the degradation efficiency [116]

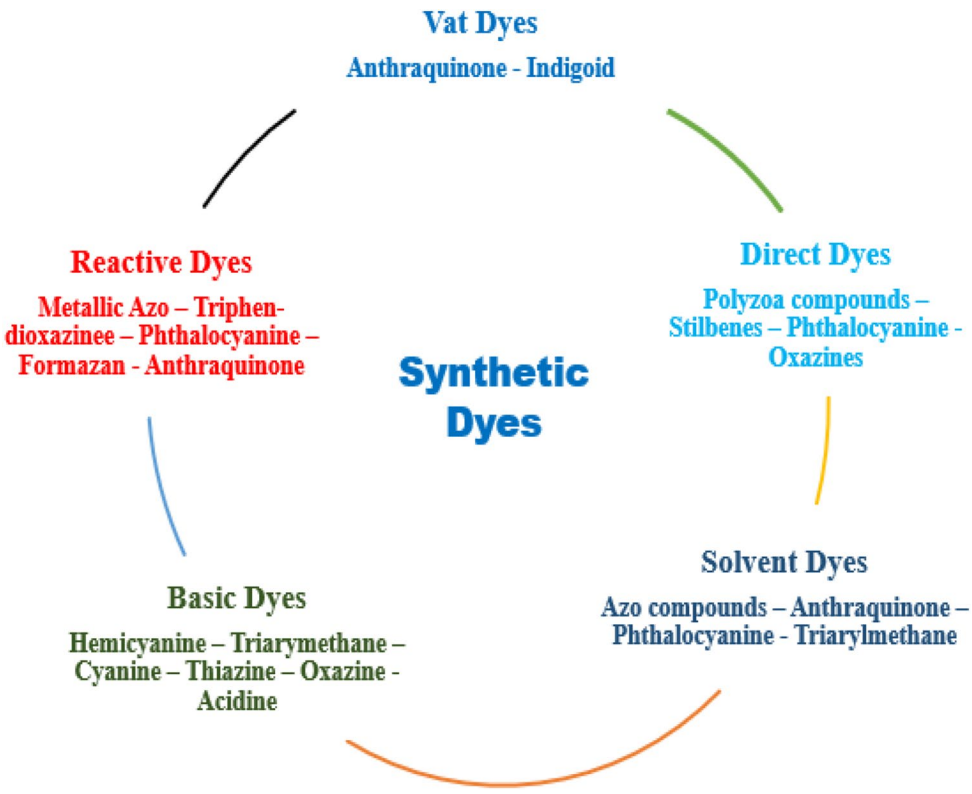

Fig. 5 Dyes classification is based on chromophore structure

are biodegradable [129]. Large numbers of semiconductors (metal oxides and complex oxides) have been examined in combination with various oxides to operate as photocatalysts for the decomposition of dyes [45, 130, 131].

Jafari et al. [132] reported nanosized TiO_2/SiO_2 immobilized on cementitious materials. Photocatalytic efficiency in removing some organic dyes was investigated. A sol–gel pioneer was initially utilized to prepare the synthesized TiO_2–SiO_2 nanoparticles characterized using UV–Vis, SEM, and XRD. A thin layer of the prepared composite was coated successfully on white Portland cement (WPC) blocks. Nano-TiO_2–SiO_2-coated WPC blocks effect was evaluated in dyes photocatalytic degradation, including MB, MG, and MO. The results indicated an increasing photocatalytic efficiency based on the composition and pH of the cement added. Khaledi Maki et al. [133] reported nanoparticles of TiO_2 doped with iron (Fe), nitrogen (N), and cerium (Ce) (Fe–N-Ce-TiO_2) immobilized on a bed of glass for organic dye degradation Direct Blue 15. The study revealed that the pH acidic condition is preferable for the removal of dye. The optimal parameters' condition for the total Direct Blue 15 dye removal under the radiation of LED is pH = 5.7, dye initial concentration 25 mg L^{-1}, dose catalyst nanoparticles 10 mg cm^{-2}, current intensity of 0.68 A (1000 lx), and contact time 60 min. Schematic of the used photocatalytic reactor used in the experiments is shown in Fig. 6.

Akerdi et al. [134] demonstrated photocatalytic removal of Acid Red 14 in an aqueous solution using nanoparticles of TiO_2 immobilized on a fabricated graphene oxide plate. The GO nanoparticles were layered on a carbon electrode (GOCE) and utilized as a catalyst bed. Nanoparticles of TiO_2 were attached to the (GO-CE-TiO_2) bed with thermal technique. For the photocatalytic procedure, a solution of 500 mL in a batch mode including dye was prepared. Photocatalytic treatment was executed for 120 min. Time effect

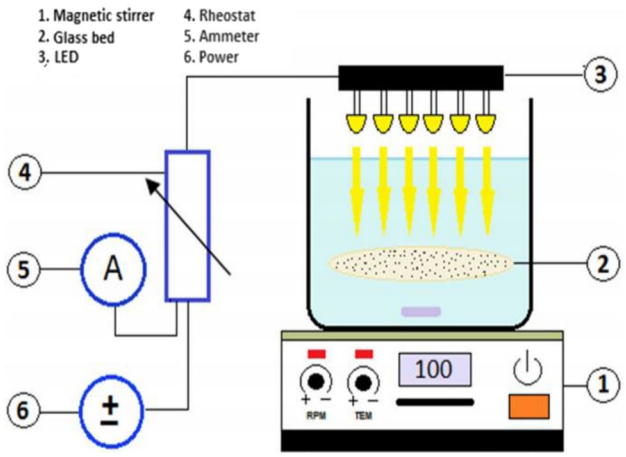

Fig. 6 Schematic of the used photocatalytic reactor used in the experiments [133]

(min), concentration of dye (mg L^{-1}), TiO_2 content (g L^{-1}), and solution pH value on the photocatalytic process were inspected. Dye removal efficiency rose in high pH (> 7) and low pH (< 7). The GO and TiO_2-fabricated electrode with (a) and the photocatalytic reactor (b) are shown in Fig. 7.

2.5 Phenolic compounds

Phenolic derivatives form a category of common recalcitrant pollutants in the environment. Their existence even at low concentrations may threaten the use or reuse of water. Phenols induce undesirable odor and taste of drinking water and have adverse effects on various biological systems. The majority of these substances are classified as toxic [135–138]. Phenolic substances are aromatic compounds bound to the aromatic ring with one or more hydroxyl groups. These substances are generally present in wastewater discharged from different industries, such as chemical synthesis, petroleum refineries, coke plants, plastics, paper, dyes, pulp, pharmaceutics, textiles, pesticides, and herbicides synthesis, as well as detergents [139–141]. Table 3 illustrates phenolic compounds successfully degraded using immobilized photocatalysis.

3 Catalyst immobilization

Recently, heterogeneous catalyst immobilization on various supports has attracted many authors because of the assumption that the catalysts could be readily isolated from the interaction solution and reused in various cycles, which reducing the expensive cost of the catalyst usage [142–144]. Supporting materials have to be inert, erosion-resistant and expose multiple areas of the surface with the capacity of holding the catalyst particles so as to remain attached and act as suspended catalysts [145]. Many researchers successfully used supporting materials such as steel mesh (SM) [146], fiberglass [147], cellulose [67], carbon fiber [148], carbon nanotube [149], silica [150].

3.1 Methods of catalyst immobilization

3.1.1 Sol–gel method

The sol–gel procedure has been widely utilized because of its many advantages, such as low cost and strong applicability to substrates. This method includes the dispersion of suspended particles in Brownian motion with a fluid matrix. The suspended particles will first transform to viscous gels before converting into solid materials [151]. A critical factor in this method is the aging time that causes the sol to freeze. This depends on the sol's concentrations, and the mechanism shown in Fig. 8 is not restrictive or

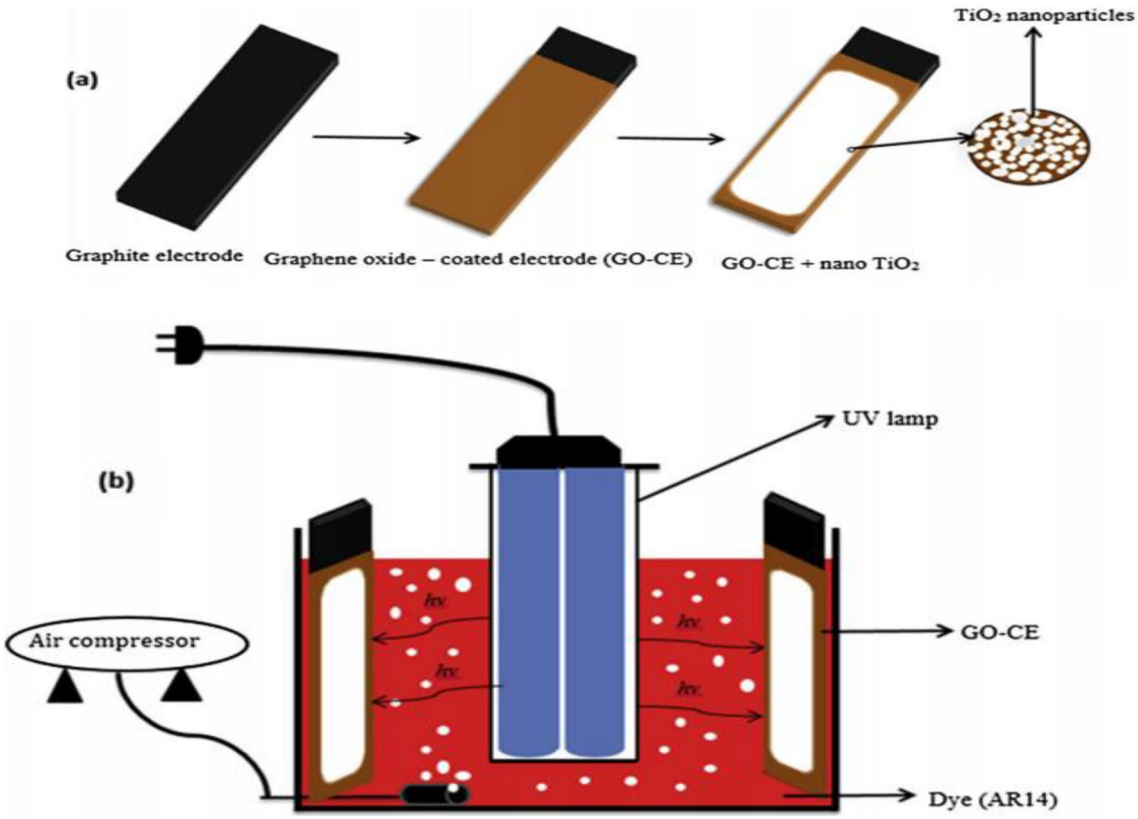

Fig. 7 GO and TiO_2-fabricated electrode (a) and the reactor of photocatalytic degradation (b) [134]

exhaustive. Such stages can be prolonged, altered, or eliminated together, except solvation and gelation; depending on a specific implementation, the steps allow for hydrolysis and condensation reactions to stay fixed to produce a sol–gel-derived material [152].

3.1.2 Chemical vapor deposition (CVD)

Chemical vapor deposition (CVD) requires a thin solid film on a substrate material by a vapor-phase precursor chemical reaction in the broadest sense. Therefore, CVD can be differentiated from physical vapor deposition (PVD), or example in terms of reactive sputtering and evaporation, involving the adsorption of atomic or molecular material on the substrate [153]. This procedure uses different energy sources such as plasma, heat, and light to deposition material. Usually, the type of gases used are chloride, hydride, and bromide. The desirable chemical composition gradient can be revealed by variation of the gas ratio, the gas's pressure, the rate of flow, deposition temperature, and type of gas [154]. CVD can be used to deposit glass/steel coating and small-scale coatings, i.e., microelectronics, on vast areas. This method provides the possibility for perfect film uniformity and controls the composition with premium phase coverage [155].

3.1.3 Electrophoretic deposition

The purpose of electrophoretic deposition is the formation of thin films for specific purposes. Under the impact of a utilized electric field, EPD includes electrophoretic motion of suspended charged particles toward an electrode and formatting of a deposit. Depending on a particulate charge, warranties can be anodic and cathodic [156, 157]. The deposition takes place depending on the type of electrode. The deposit occurs on the cathode when the particles are positively charged, and the operation is called cathodic electrophoretic deposition. The process is called anodic electrophoretic deposition when the deposit occurs on the positive electrode (anode) of negatively charged particles [158]. Figure 9 illustrates the schematic diagram of EPD [159]. In EPD, a current flows between the parallel sheets' electrodes when a potential is applied. The magnitude of the flowing current is determined by several device parameters involving cell constant, electrochemical kinetics, and solution conductivity [160]. EPD has recently been used to manufacture composite and functional ceramics, thin films, coated and functionally graded substances, high-performance ceramic, hybrid coatings; and biomaterials and to deposit carbon nanotubes and nanoparticles in the manufacture of developed nanostructured materials [161].

Table 3 Phenolic compounds successfully degraded using immobilized photocatalysis

Phenolic compound	Catalyst	Support	Experimental conditions	Main outcomes	Reference
Phenol, M-cresol, Resorcinol	TiO_2	Mesoporous carbon (CMK-3)	Operating conditions: UV light irradiation 150 W, room temperature, initial pH ranged from 4 to 10, initial concentration of TiO_2/CMK-3 varied from 0.05 to 0.5 g L^{-1}, reaction time varied from 30 to 150 min, the concentration of phenolic compound varied from 50 to 200 mg L^{-1},	The highest removal of TOC for resorcinol phenol and m-cresol was observed to be 78%, 74%, and 62%, respectively. Optimum conditions: TiO_2/CMK-3 initial concentration 0.15 g L^{-1}, Initial concentration of phenolic compound 100 mg L^{-1}, pH = 6, and 150 min for irradiation time	[241]
Phenol	$CuFe_2O_4$	rGO	Operating conditions: Initial concentration of phenol 200 mg L^{-1}, 95 mL phenol solution, 5 mL H_2O_2 30% conc., initial concentration of $CuFe_2O_4$/rGO 60 mg, 400 W UV illumination lamp, pH ranged from 3 to 10,	Complete removal for phenol at optimum conditions: 150 min, pH 3,	[242]
2,6-Dimethylphenol	CuO	Clinoptilolite nanoparticles (NC)	Operating conditions: Initial concentration of CuO in composite varied from 3.52 to 6.18%, initial concentration of CuO–NC varied from 0.1 to 0.4 g L^{-1}, initial concentration of DMP varied from 20 to 40 mg L^{-1}, Hg lamp 35 W,	Best DMP degradation at CuO amount 6.18% in the total composite CuO/NC, CuO–NC concentration 0.25 g L^{-1}, DMP concentration 30 mg L^{-1}, illumination time 300 min, pH 5.5	[243]
Phenol	TiO_2, ZnO	Activated carbon (AC)	Operating conditions: UV lamp 8.1 W, temperature 32 °C ± 3, time 240 min, catalyst dose varied from 0.1 to 1 g L^{-1}, initial concentration of phenol ranged from 10 to 100 mg L^{-1}	100% phenol degradation at phenol initial concentration of 10 mg L^{-1}, time 120 min, catalyst dose 0.1 g L^{-1}, ZnO showed higher efficiency than TiO_2,	[244]
Phenol	Fe_3O_4-doped OMC	Sintered metal fibers	Operating conditions: stainless steel reactor, T 80 °C, initial concentration of phenol 1 g L^{-1}, initial concentration of H_2O_2 5.1 g L^{-1}, flow rate 2 mL min^{-1}	100% phenol degradation after 3 h	[245]

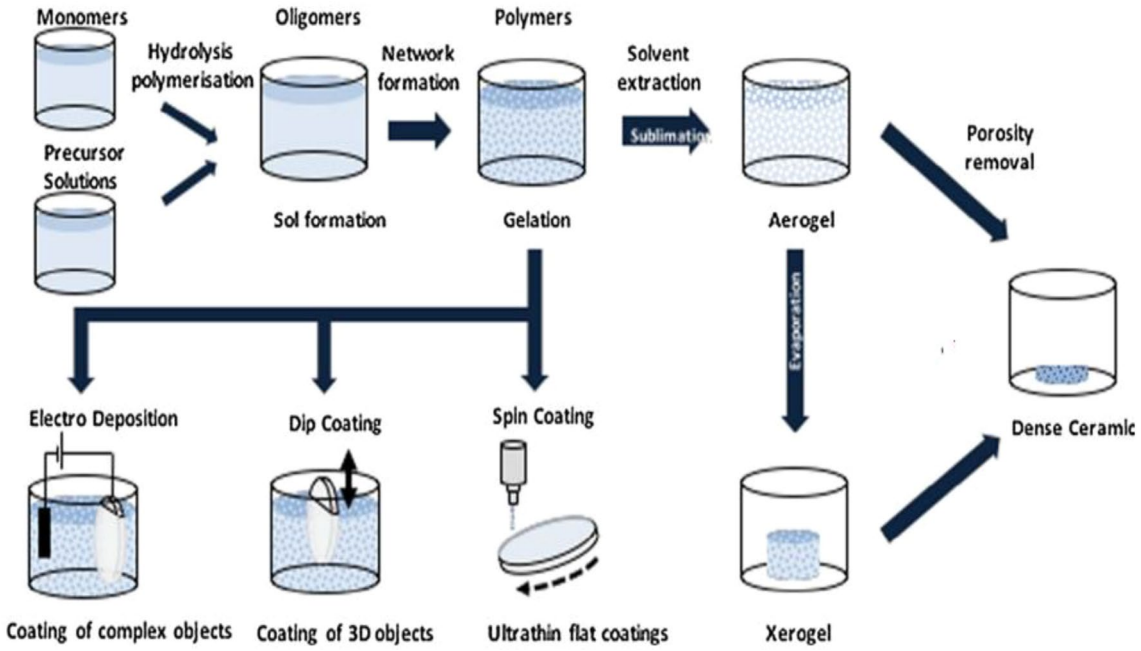

Fig. 8 Routes of syntheses of sol–gel. Procedures are characterized by the transfer of colloidal solution to an interconnected network (gelation) as a sol–gel procedure [152]

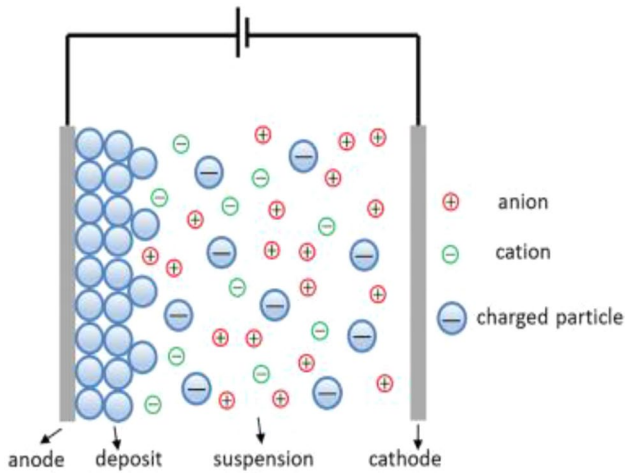

Fig. 9 Electrophoretic deposition process schematic illustration [159]

3.1.4 Plasma-sprayed coating technique

The plasma spraying procedure can be outlined as follows: firstly, the precursor solution of the metal or ceramics is heated via an ionized inert gas (plasma); then, the heated compounds are sprayed at the desired surface for coating, in general, a metallic alloy or metal. This procedure is generally utilized for providing a barrier against corrosion, wear, or high temperatures [162]. The porous structure of the coatings required for catalytic implementations in plasma spraying depends significantly on the jet outflow regime (turbulent, laminar, or transient), the flow rate, and components of the plasma-forming gas, spraying distance, the applied power, and the average bulk temperature [163].

3.1.5 Magnetron sputtering deposition

Magnetron sputtering is a plasma-based procedure that is ionized. It accelerates inert gas (usually Ar) atoms that are ionized and accelerated because of the possible difference between the anode and the negatively biased target (cathode). The interactions between the ions and the desired surface enable atoms to be ejected (sputtering), condensing on a substrate and forming a film [164]. When the sputtered atoms move via the thick plasma, the probability of an ionizing collision is significantly higher than in a conventional discharge of magnetron, where far more particles move to the substrate without collisions, shields, walls, or other components. The target requires good electrical conductivity to facilitate the high-current pulses [165].

3.2 Advantages of catalyst immobilization

It is possible to use catalysts either in immobilized or suspended form. After dispersing the used catalyst particles in the aqueous solution, the illumination's penetration deepness is restricted due to scattering or absorption through the dissolved organic matter and

catalyst particles [145]. Unsupported catalysts are often less stable, and as a rule, coagulation is inevitable through the catalytic reactions [166]. In large-scale systems, the usage of unsupported catalysts involves a time-consuming, expensive process for the isolation from the treated wastewater before disposal and recycling of the catalyst. The photocatalyst immobilization can obviate the above drawbacks given over appropriate support [167]. For instance, the TiO_2 catalyst is usually utilized in suspension (slurry) with premium performance; however, costly filtration is needed to isolate the treated solution's catalyst [168, 169]. Table 4 briefly lists the benefits and drawbacks of suspended and immobilized photocatalysts [31].

4 Supporting materials

The materials used for immobilization are named support, carrier, or anchored materials. The material's properties are significant in revealing the success of immobilization. Supporting materials should possess the following qualities [170]:

- Low cost and eco-friendly material.
- Static after immobilization process and does not obstruct the required reaction.
- Resistance in mechanical and thermal properties.
- High constancy versus degradation by vigorous oxidative radicals produced via the photocatalyst when its surface is illuminated.
- The material must be strongly anchored with the catalyst, even after entering the reactor.
- Catalyst activity must not be positively affected after immobilization.
- It provides a high surface area for the catalyst.
- High durability.

The support material's primary function is to enhance the contact mass's textural properties (excess surface area, porosity, etc.) [171]. Supports are usually categorized as organic and inorganic supports by their chemical nature. Whatever the support, it plays a significant part in active catalyst immobilization. There are three main functions of the support: (i) to expand the catalytic material surface area; (ii) to reduce sintering and enhance the catalytic material's hydrophobicity and thermal, hydrolytic, and chemical stability; (iii) to regulate the beneficial lifetime of the catalyst [172]. In this review, we will divide support materials into two categories: movable and fixed supporting.

4.1 Movable supporting materials

Movable supporting means that the catalyst is attached to the supporting material and acts as one group when placed into the aqueous media to improve the catalyst activity. The advantage of this type of support is the same for suspended catalysts, such as the high interaction surface area, which participates in the superior degradation of contaminates [173].

Table 4 Benefits and drawbacks of suspended and immobilized photocatalysts [31]

Suspended type photoreactors	Immobilized photoreactors
Benefits	*Benefits*
Catalyst distributed uniformly	Continuous operation of the reactor
Significant photocatalytic illumination surface area to reactor volume ratio	Superior elimination of organic matter from the aqueous phase while using an immobilized agent with adsorption characteristics
Mass transfer is limited	No additional catalyst separation operation required
Because of catalyst continuous adding and removing, the catalyst fouling effects are extremely minimized	
Particles mixed as well	
Low-drop in pressure through the reactor	
Drawbacks	*Drawbacks*
Post-expensive filtration processes are required	Lower operation efficiencies by immobilized photocatalyst due to light scattering
Effective light dissipation and adsorption in the suspended particles medium	A possible limitation of mass transfer at minimal flow rates of the contaminates
	Possible catalyst washout and catalyst deactivation

4.1.1 Zeolite

Zeolites are defined as microporous-crystalline aluminosilicates. They have been formed by sharing the corner AlO_4^- and SiO_4^- tetrahedra [174, 175]. Zeolites are low cost, friendly to the ecosystem, and renewable. They are potentially valuable resources to remediate cumulative contaminates. Natural zeolite has many mesoporous structures (distribution of pore size varying from 2 to 50 nm), including broad internal and external cation adsorption surface active sites [176–179]. Due to their adsorption ability, zeolites have attracted greater attention, helpings to collect the contaminates to the catalyst surface's closeness, leading to rapid removal [180].

Danish et al. [181] demonstrated ultra-fine nanoparticles of iron–nickel bimetallic. These nanoparticles are immobilized on natural zeolite composite (Z-nZVI-Ni) as a heterogeneous catalyst for trichloroethene degradation (TCE). The results demonstrated that the combination of nickel and iron particles on the zeolite plate dramatically increased the BET's surface area to 120 $m^2.g^{-1}$. By increasing nickel from 1% to 5% by weight in the Z-nZVI-Ni, the TCE removal was completely achieved. Leal Marchena et al. [182] studied tungstosilicic acid (TSA) anchored on NH4Y and NH4ZSM5 zeolites, which were successfully synthesized by wet impregnation for MO photodegradation. The increase in TSA amount on the zeolite produces a persistent boost in photocatalytic action and degradation rate. The catalyst quantity's optimum concentration was 0.5 g L^{-1}; however, increasing the catalyst quantity reduces the removal rate because the solution becomes opaque and cloudy, decreasing light penetration. Liao et al. [183] demonstrated an enhanced zeolite/TiO_2 composite (MZTC), which was synthesized *in situ* using a saturated infiltration method. The photocatalytic efficiency of MZTC was estimated under UV light irradiation by examining the rate of degradation of (MB) dye in an aqueous solution. The test's degradation efficiency detected that MB's degradation by MZTC-2.5 composite was the maximum, reaching 93.6% within 60 min. Figure 10 shows a schematic of MB degradation using MZTC-2.5 [183]. Ajoudanian et al. [184] studied nickel oxide (NiO) incorporated into clinoptilolite (CP) zeolite nanoparticles. Ion exchange and calcination techniques were performed. The immobilized catalyst was characterized by SEM, TEM, DRS, FT-IR, XRD, and BET. The developed catalyst was used in cephalexin (CEX) photocatalytic degradation. The optimum experimental conditions were catalyst initial dose 0.2 g L^{-1}, pH 4.5, and 300 min of irradiation time. At this optimal status, up to 76% of CEX was degraded.

4.1.2 Polymers

Polymers have achieved an excellent position due to their intrinsic properties, among other materials [185]. They are used to produce manufactures such as lami-

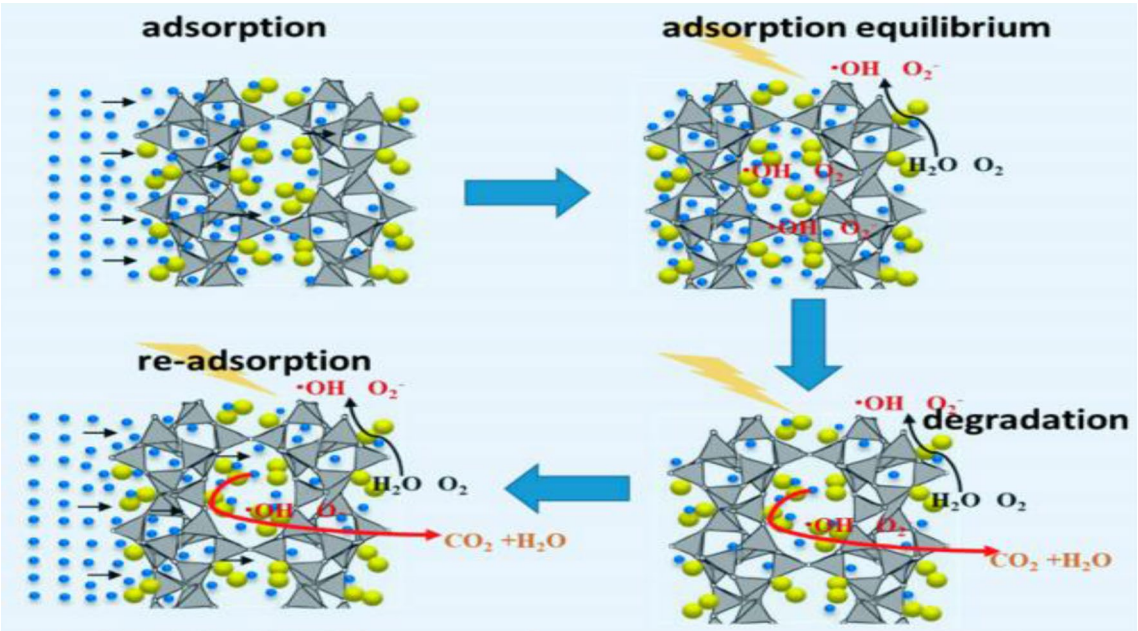

Fig. 10 Schematic of the degradation of MB using MZTC-2.5 [183]

nates, paints, plastic sheets, building materials, household appliances, and packing [186]. Immobilizing the catalysts on polymers negates the need for separation procedure after water treatment and eliminates ecotoxicity-related problems [187]. Use of polymers as the carrier for TiO_2-based photocatalysts is common. These polymers include polysulfone, polyethersulfone, polyamide, cellulose acetate, polyacrylonitrile, polyvinylidene fluoride, and polypropylene [188]. According to Singh et al., polymers are suitable for catalyst immobilization for the following reasons [170]:

- They are innoxious substances that are completely inert and have high durability, and are mechanically stable.
- They have hydrophobic properties, which give them additional advantages.
- They are readily available and costless
- Thermoplastic properties boost the ease of coating the catalyst by thermal methods.
- They have high resistance to UV irradiation and do not oxidize quickly

Jallouli et al. [189] reported paracetamol photocatalytic degradation. Nanoparticles of TiO_2 and TiO_2/cellulosic fiber were examined under sunlight and UV irradiation. TiO_2 suspension/UV technique showed extra efficiency than the TiO_2/cellulosic fiber technique. However, immobilized TiO_2 showed several advantages over the suspended system. It can improve the adsorption properties while permitting the photocatalyst to be easily separated from the solution with enhanced reusable performance. Aoudjit et al. [190] demonstrated the usage of TiO_2 (P25) nanoparticles supported into a poly (vinylidene fluoride–trifluoroethylene) (P (VDF–TrFE)) membrane. The synthesized membrane was used in tartrazine dye photocatalytic degradation. The results showed that 8 wt. %. TiO_2 nanocomposite has a noticeable sunlight photocatalytic action over about 5 h. The degradation efficiency reached about 78% of contaminates.

4.1.3 Quartz sand

Silica crystals (SiO_2), the main composition of quartz sand material, are other impurities that we removed through the deposition procedure. Quartz sand, otherwise recognized as white sand, is weathered rocks, including feldspar and quartz. The quartz sand's main composition is Al_2O_3, SiO_2, TiO_2, Fe_2O_3, MgO, CaO, and K_2O [191]. He et al. [192] demonstrated the impact of solar irradiation on wastewater, including PhACs, by employing immobilized TiO_2 that exist as a catalyst and studied the prospect of this photocatalysis as a post-treatment procedure effluent of wastewater. Experiments were carried out using supported TiO_2 (photocatalysis) and without (photolysis). Firstly, using a sol–gel technique, on 200–500 µm sand, TiO_2 was successfully immobilized. The photocatalysis result is significant in the complete removal of PhACs in wastewater effluent. For diclofenac, propranolol, and carbamazepine, $76 \pm 3\%$ was the removal efficiency. Ben-Moshe et al. [193] reported quartz sand as support for copper oxide nanoparticles and their catalytic efficiency to decompose an organic dye. Supported sand was filled in a column for studying the catalytic action for the decomposition of Lissamine green B organic dye through experiments with an oxidant hydrogen peroxide. A promising consequence was shown for the CuO catalyst when used in a suspended form in batch systems. The impact of nanoparticle immobilization on quartz sand and its inclusion in the catalytic procedure have been studied in a flow-through apparatus. For organic dye degradation, the covered sand was filled in a column, and its catalytic efficiency was studied with an oxidant such as hydrogen peroxide. Configuration trials with uncovered sand were likewise carried out for comparison. The covered sand reported a significant catalytic potency, reaching total oxidation of the dye. The removal was enhanced by extending the dye's residence time in the column, yielding removal of the dye up to 85%. For organic dye degradation, the covered sand was filled in a column, and its catalytic efficiency was studied with an oxidant such as hydrogen peroxide. Configuration trials with uncovered sand were likewise carried out for comparison. The covered sand reported a significant catalytic potency, reaching total oxidation of the dye. The removal was enhanced by extending the dye's residence time in the column, yielding removal of the dye up to 85%.

4.1.4 Three-Dimension graphene

Over the last few years, three-dimensional graphene-based materials (3D GBMs) have increasingly attracted concern. While they preserve the outstanding graphene properties, they also improve the functional application potential of graphene. The manufacture of 3D graphene is mostly conducted by methods of template-assisted chemical, chemical self-assembly, and chemical vapor deposition (CVD), as shown in Fig. 11 [194].

He et al. [195] studied a three-dimensional graphene hydrogel-AgBr@rGO to degrade bisphenol. This research discusses the encapsulation of AgBr to create a composite (AgBr@rGO) by reduced graphene oxide, which can be combined from three-dimensional (3D) network structures with hydrogels (rGH-AgBr@rGO). AgBr@rGO's core–shell design inhibited AgBr particle growth, and excellent size control (500–600 nm) was achieved; however, hybridization with graphene developed quick migration and separation of photogenerated charges. rGH-AgBr@rGO's 3D graphene nanosheets quickly adsorbed bisphenol A (BPA). BPA was

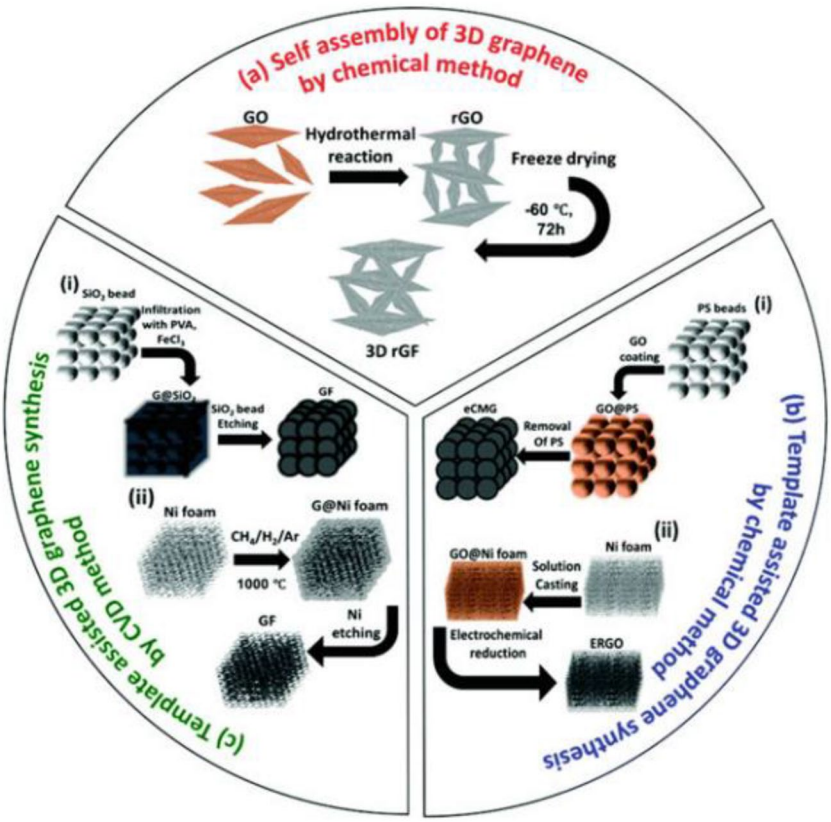

Fig. 11 Fabrication methods for 3D graphene [194]

then quickly decomposed by AgBr@rGO nanoparticles under visible light irradiation. The results indicate that the interconnectedness between adsorption and photocatalytic decomposition could considerably enhance the degradation efficiency of pollutants. A regenerated micron-sized 3D mesh is structured via a simplistic filter without the requirement for complicated catalyst filtration. The data acquired showed excellent interconnectedness between the adsorption-based pollutant and photocatalytic decomposition by rGH-AgBr@rGO. 150% BPA removal was more significant than pure AgBr, and after five consecutive cycles, about 90% removal efficiency was achieved. The complete degradation of BPA was achieved through the first 6 h. Nawaz et al. [196] studied a synthesized three-dimensional (3D) reduced graphene oxide/TiO_2 (RGOT) aerogel, which was synthesized by a simplistic hydrothermal one-step procedure. The photocatalytic assessment of carbamazepine (CBZ) recalcitrant substance in an aqueous solution was evaluated. RGOT revealed superiority in adsorption and about 200% greater photodegradation efficiency than pure TiO_2 (of more than 99%), with 90 min CBZ elimination observed in 10 ppm aqueous solution. CBZ adsorption and photocatalytic degradation are significantly affected by the TiO_2 mass ratio in RGOT aerogel; the optimal TiO_2/GO in RGOT was found to be 2:1. The attractive benefits of RGOT aerogels are many, including its macroporous 3D structure, effective charge separation, considerable surface sites for immobilizing the catalyst, and CBZ mass transportation near the photocatalyst surface area.

4.1.5 Other uncommonly used supports

Besides these prevalent supports, there are abundant other unusual supports, including those based on sodium alginate [197], cellulose acetate [198], and laccase enzyme [199], which have been used for the immobilization of the photocatalytic material. Ye et al. [200] reported phenol degradation using synthesized ZnO nanosheets/Montmorillonite photocatalyst. The composite was produced without calcining via the novel in situ alkaline hydrolysis syntheses method. The phenol's efficient degradation via the composites reached 88.5%, which is higher than the ZnO photocatalyst (56%).

4.2 Fixed supporting materials

For large-scale industrial purposes, immobilized photocatalysts on fixed support materials are greatly preferred, because there is no requirement for a filtration unit at the end of the treatment process. Initial and running costs are reduced, making the system further commercially viable for a large industrial scale. Fixed support materials also

have their drawbacks; the main reason for the decrease in efficiency is the reduced surface area, which reduces the degradation rate. Thus, it is necessary to prolong photocatalytic treatment time, reducing the treated substratum's daily capacity [147].

4.2.1 Glass plates

Due to their UV light transparency in photocatalytic applications, the glass plates are appropriate as catalyst support. As a result, this can offer a considerable surface area and expand the efficiency of photocatalysis. Moreover, extra potential benefits such as additional surface area improved adsorption characteristics and improved reduced recombination of charge or surface $^{-}$OH groups in photocatalysis [201]. Darvishi Cheshmeh Soltani et al. [202] demonstrated the photocatalytic technique usage fitted with nanoparticles ZnO immobilized on glass plates for removal of formaldehyde in aquatic solution. The efficiency of formaldehyde degradation reduced significantly to 12.96% because the solution had a heavy, strong acid condition (pH = 2.0). The efficiency of degradation was reduced from 56.41 to 44.02% by raising pH values from 7 to 10, respectively; a significant decrease in the degradation efficiency was shown at basic status. When the initial formaldehyde concentration supplied inside the reactor rose from 500 to 4000 mg L^{-1}, the degradation efficiency reduced from 62.30 to 11.96%, respectively, in 30 min. The result suggests that the photocatalytic technique using immobilized ZnO nanoparticles could be an effective and promising tool for wastewater treatment, including formaldehyde.

Maleki et al. [203] demonstrated ZnO nanoparticles prepared and immobilized on glass plates through chemical precipitation techniques for humic substances (HS). The initial concentration of (HS), pH effect, surface area, and UV lamp power were the studied parameters. Acidic conditions preferred the photocatalysis of HS. Increasing the power of the UV lamp and the glass surface area enhanced HS's degradation efficiency. Jafari et al. reported toluene and benzene oxidation by nanoparticles of ZnO, which were immobilized using the photocatalytic techniques on glass plates. Nanoparticles of ZnO were coated with a heat attachment method on three glass plates. To estimate the photocatalytic degradation efficiency of toluene and benzene, a layered plate was illuminated by a metal halide lamp in a reactor with a rectangular shape in batch mode. Glass surfaces coated with ZnO suspension achieved 57% and 46% degradation of toluene and benzene when concentration was 50 ppm at 45 °C and relative humidity of 40% after 240 min illumination of metal halide lamp. Shokri et al. [204] demonstrated cefazolin photodegradation in the existence of TiO_2. TiO_2 was examined as immobilized on glass plates and in suspended form. The initial concentration of cefazolin, initial pH of the solution, catalyst dosage, and light intensity were the observed operational parameters. The best conditions achieved for the photodegradation of cefazolin were pH 5, an initial concentration of cefazolin = 20 mg L^{-1}, with light intensity of 17 $W.m^{-2}$ in both cases.

4.2.2 Aluminum plates

Research on aluminum sheets is still limited and needs further study, despite several successful attempts, presented in the following lines. Gar et al. [205] demonstrated a recycled photocatalyst produced by incorporating sulfur cations into the lattice of titanium dioxide (TiO_2) with a highly active visible light. Aluminum plates were used as a support material for the prepared photocatalyst. Polysiloxane was used as the attaching material for cyclic use in photocatalysis experiments. Degradation of 2,4-dichlorophenol (2,4-DCP) was successfully achieved using suspended and immobilized catalysts under a direct illumination of a metal halide lamp. Removal of 2,4-DCP by the suspended catalyst, by comparison, was more rapid than by the immobilized catalyst. On the other hand, the immobilized catalyst trends in removal rates denote that the degradation of 2,4-DCP could be prolonged for extra time to achieve the same efficiency as the suspended catalyst. For an initial concentration of 25 mg L^{-1}, the result of degradation was higher than 97% after 480 min for 2,4-DCP. Degradation rates were 98%, 96%, 90%, 86%, and 80.4% in five consecutive cycles, resulting from the significant catalyst stability and the possibility for reusability even after long periods of photocatalytic reaction.

Seabra et al. [206] reported active layers of TiO_2 immobilized on aluminum sheets, using a jet spray, a conventional and low-cost deposition process. The layers attached to the substrate were carried out using a commercial thermally adherent polyester ink used in industry for aluminum surface treatment. The layers' photocatalytic efficiency was examined to remove Orange II organic dye in aqueous solutions. The reaction was examined in a batch photoreactor under solar and visible light. The attached catalysts were compared with suspension TiO_2 (anatase). For a TiO_2 and polyester ink layer having a 1:1 weight ratio and a thickness of 60 m (100 g m^{-2}), the enhanced achievement was reached for layers. These layers confirmed attracting discoloration performance degree of 95%.

4.2.3 Stainless steel

Stainless steel is efficient as a substrates for TiO_2 because: it is low cost, high strength, and chemically and thermally stable. Mirzaei et al. [207] demonstrated a spinning stainless steel disk photoreactor by immobilizing TiO_2 on the disk surface; the degradation of phenol was studied in aqueous solutions. The completed degradation predicted for phenol

was 100% at the optimum condition (flow rate 2000 mL. min^{-1}, rotational speed 290 rpm, and disk diameter 22 cm). Murgolo et al. [208] studied a TiO_2 nanostructured film placed on a stainless steel mesh via the Metal–Organic Chemical Vapor Deposition (MOCVD) procedure. Trimethoprim and warfarin degradation was twice with the new catalyst as when using TiO_2 Degussa P25. K. Fouad et al. [209] demonstrated a novel engineering-designed photocatalytic reactor. The reactor was used for the repetitive degradation of sulfamethazine (SMZ). Tungsten-doped TiO_2 (W-TiO_2) catalysts were immobilized into four consecutive stainless steel plates by using polysiloxane. Under the optimum operating conditions, the SMZ concentration residual after 30 min of the photocatalytic reaction was below the detection limit. The immobilized W-TiO_2 catalysts showed high stability even after five consecutive runs. The photocatalytic reactor is shown in Fig. 12.

4.2.4 Other uncommonly used materials

Verma et al. [210] used supported TiO_2 on cement beads for an imidacloprid insecticide (IMI), as shown in Fig. 13, involving degradation with durability examination of the catalyst. In suspension mode, running conditions were optimized for the superlative degradation by varying pH, the dose of H_2O_2, TiO_2, and the batch reactor area/volume ratio. After photocatalytic treatment of up to 3 h, about 95% of IMI was degraded under all optimized conditions. In a fixed-bed analysis, the degradation of IMI was employed using TiO_2 coated cement spherical beads. The spherical beads' diameter was about 2.0 cm with two coatings of the catalyst, sufficient for removing IMI after 6 h. The performance and stability of the anchored catalyst were tested 30 times by recycling the beads.

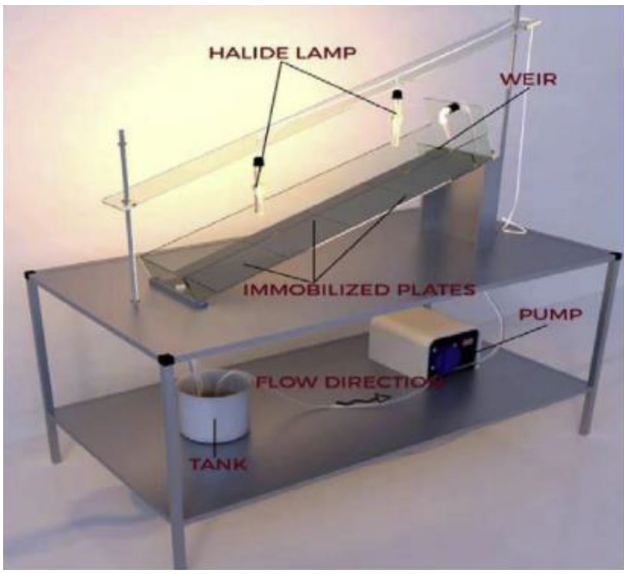

Fig. 12 Perspective sketch for the photocatalytic reactor [209]

Fig. 13 Supported TiO_2 on cement beads [210]

5 Photocatalytic reactors

Photocatalytic reactors are classified into two classes based on photocatalyst conditions: reactors that have photocatalyst immobilized on a surface, and reactors whose photocatalyst is in the suspended form [211]. The significant advantage of immobilized reactors is that they allow continuous operation, have no need for catalyst particle separation, and may reuse catalytic supports for various cycles. The main disadvantages of surface-immobilized reactors are the low area-to-volume ratio, leading to mass transfer restrictions and low reaction rates. However, suspended reactors have a high specific surface area of suspended catalytic particles [212]. For water purification and wastewater treatment, a photocatalytic reactor can be a perfect solution.

5.1 Movable supported photocatalytic reactors

A reactor that consists of TiO_2 immobilized on glass beads and has in the center a UV lamp was used for degradation of high ammonia in water [213]. Zhong et al. [214] reported pumice-loaded CeO_2/Bi_2WO_6 photocatalysts using macroporous pumice as support. SEM images indicate that pure pumice is a porous substance with a smooth surface and relatively large pores, In contrast, pumice in pumice-loaded CeO_2/Bi_2WO_6 catalysts has very rugged textures and clings to them with a layer of catalyst films on surfaces. A photoreactor with a continuous flow with dimensions $410 \times 60 \times 200$ mm, composed of a settling tank and three reaction tanks was used.

Volume was 0.8 L for reaction tanks, and a 100 W lamp was used for illumination. Claes et al.[215] illustrated a photocatalytic reactor for the degradation of MB dye. A reservoir was equipped with a peristaltic pump to supply the reaction solution to the reactor containing methylene blue trihydrate. An LED array was linked to movable pillars to provide a light source at a distance of 4 cm from the reactor. TiO_2 was coated over borosilicate beads and was situated in the middle part. The experimental setup is shown in Fig. 14 [215].

5.2 Fixed supported photocatalytic reactors

Zhang et al. [216] demonstrated a fixed-bed reactor designed by immobilizing a thin film of BiOI on glass fiber cloth (GFC); the fixed-bed reactor is shown in Fig. 15. It consists of a light source, two reservoirs, a peristaltic pump, and a sloping plate to support the film and collection of light. The reactor's photocatalytic action was examined by bisphenol A (BPA) degrading under a sunlight simulator. BPA's initial concentration (20 mg L^{-1}) was degraded up to 98% by the BiOI thin-film reactor within 8 hs' irradiation and pH range (5–9). O'Neal Tugaoen et al. [217] studied the degradation of para-chlorobenzene acid (pCBA) using a TiO_2-coated quartz optical fibers reactor, as shown in Fig. 16. The photoreactor contains a Clear PVC cylinder with an inner diameter of 1.9 cm and a total length of 18 cm. 16 cm was the solution depth, with a 5 $ml.min^{-1}$ flow rate using a peristaltic pump. The highest degradation was achieved by utilizing five coated fibers with five LEDs [217].

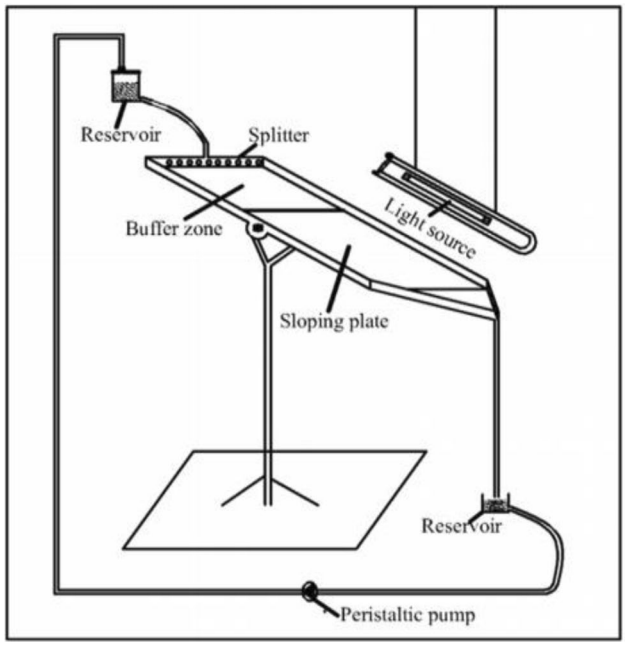

Fig. 15 Thin-film fixed bed reactor [216]

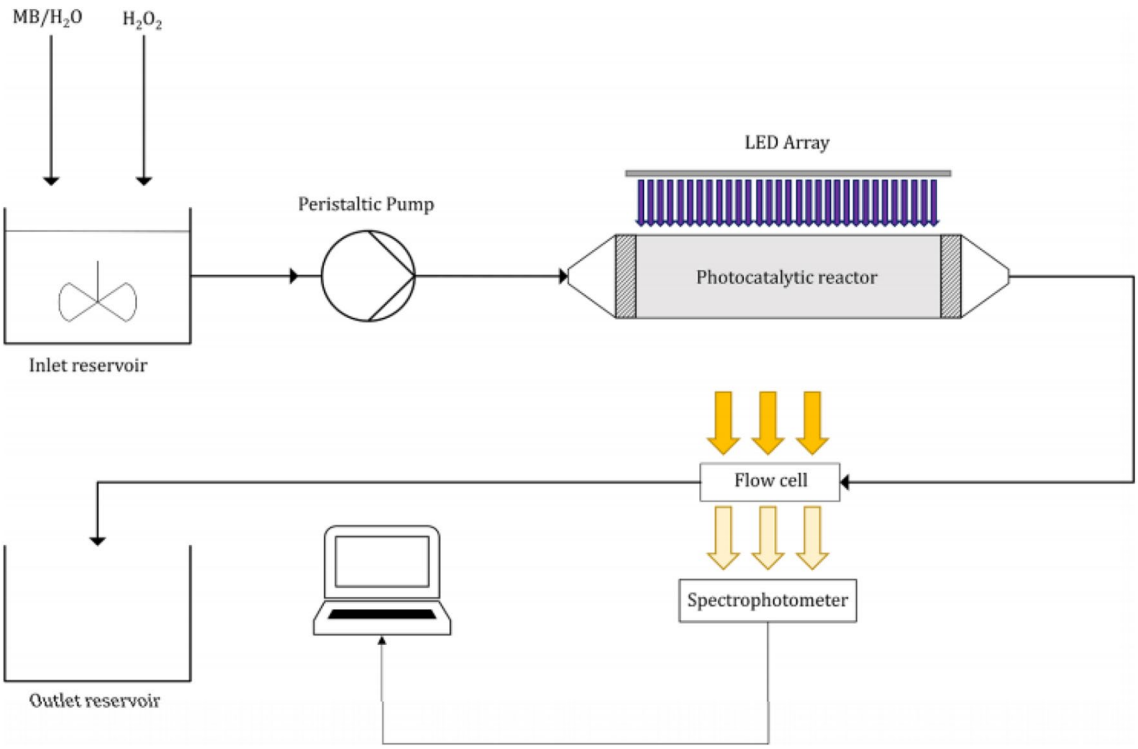

Fig. 14 Experimental setup schematic for TiO_2 coated over borosilicate beads [215]

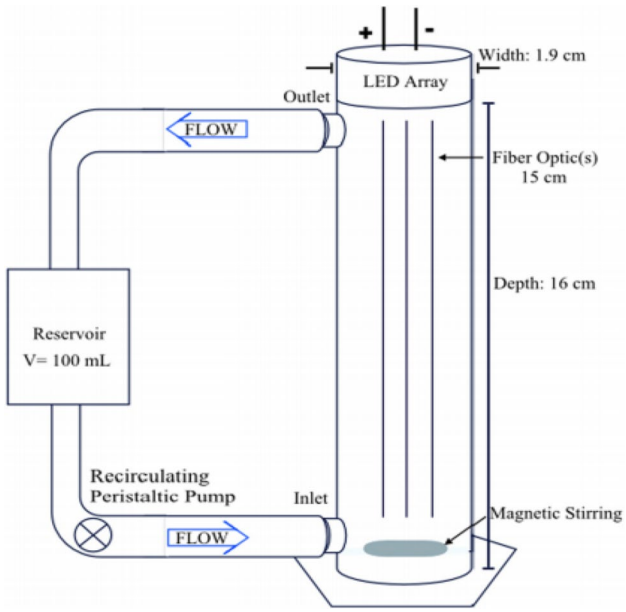

Fig. 16 OF/LED photocatalytic reactor [217]

6 Reusability of catalysts

The reusability of the attached catalyst is an essential point. It depends on the method of attaching on the catalyst itself. Degradation efficiency illuminates at last runs due to the effect of scouring, which induces particles that are not well immobilized to desolate the supporting material because of the shear force generated by the rapid movement of polluted solution. Gar et al. [205] degradation of 2,4-dichlorophenol in water using the photocatalytic technique was tested on aluminum plates, using a reusable immobilized S-TiO_2 by polysiloxane. The experimental tests were carried out over longer periods (480 min) and under the same circumstances, s, as shown in Fig. 17. After five repeated runs, the final degradation efficiencies were 98%, 96%, 90%, 86%, and 80.4%, respectively. The removal of the repetition periods' displays high catalyst performance and constancy despite long durations of the photocatalytic procedure.

7 Conclusions

There is no doubt that high pollution rates, especially from recalcitrant organic pollutants, mean we face major challenge because these pollutants will return to us in one form or another. The researchers spared no effort to find safe and economical methods of treatment. The trend in recent years is strongly toward AOPs techniques. This method is effective, but not practical if used in suspended form on a large scale. Hence, using this technique in immobilized form is the optimum way forward. This review specifically covered classes of recalcitrant organic pollutants, the possibility of the degradation of such pollutants using immobilized photocatalysis, photocatalytic reactors, and reusability of immobilized catalysts.

Study recommendations could be as follows:

1- The use of suspended catalysts is effective only in laboratory experiments or preliminary studies; however, it is not appropriate to apply on an industrial level.
2- Immobilized photocatalysts are applicable in reactors, which could be utilized as a unit in wastewater treatment plants or for special effluents. They could solve the problems of suspended form, such as cost and difficulty of reuse.

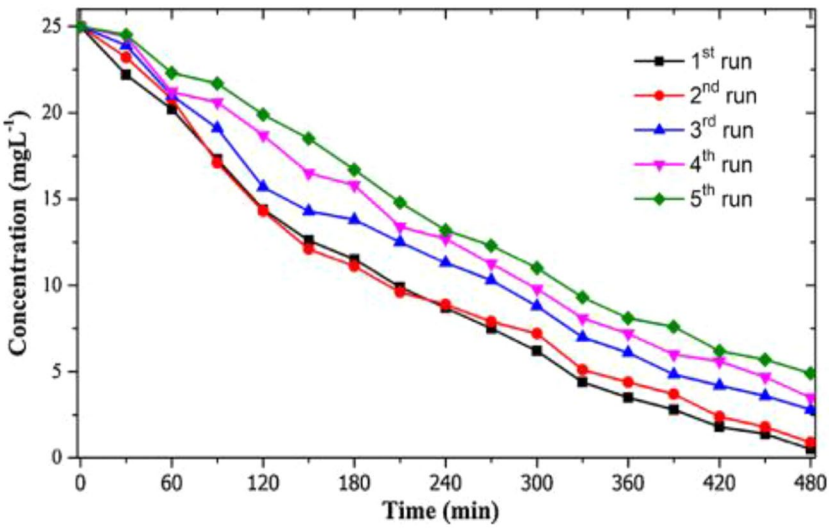

Fig. 17 Reusability of immobilized catalyst, initial concentration of 2,4-DCP 25 mg L^{-1} [205]

3- Studies on the treatment of pesticides using immobilized photocatalysis need to be increased, as there has been a lack of studies dealing with pesticides.
4- The degradation of surfactants needs further study, especially since it is used extensively in all fields.
5- The use of immobilized photocatalytic reactors should be encouraged, because they are the future and the possibility of using them as additional units in the stations.
6- Estimation of cost of reactor's is crucial when evaluating the benefits of these reactors.
7- The immobilized photocatalysts' performance cannot be evaluated without evaluating the possibility of reuse of immobilized catalysts for long periods.

Acknowledgements The second author would like to acknowledge the assistance provided by the Science and Technology Development Fund (STDF) for funding the project, No. 41902 (Center of Excellence in Membrane-based Water Desalination Technology for Testing and Characterization".

References

1. M. Bassyouni, A.E. Mansi, A. Elgabry, B.A. Ibrahim, O.A. Kassem, R. Alhebeshy, Appl. Phys. A Mater. Sci. Process. **126**, 38 (2020)
2. Y. Zhang, X. Xiong, Y. Han, X. Zhang, F. Shen, S. Deng, H. Xiao, X. Yang, G. Yang, H. Peng, Chemosphere **88**, 145 (2012)
3. K. Fouad, M. Gar Alalm, M. Bassyouni, M. Y. Saleh, Environ. Technol. Innov. **23**, 101778 (2021)
4. Z. Sabouri, A. Akbari, H.A. Hosseini, A. Hashemzadeh, M. Darroudi, J. Mol. Struct. **1191**, 101 (2019)
5. H. Wang, N. Wang, B. Wang, Q. Zhao, H. Fang, C. Fu, C. Tang, F. Jiang, Y. Zhou, Y. Chen, Q. Jiang, Environ. Sci. Technol. **50**, 2692 (2016)
6. W. Da Oh, T.T. Lim, Chem. Eng. J. **358**, 110 (2019)
7. D. Li, Q. Zhu, C. Han, Y. Yang, W. Jiang, Z. Zhang, J. Hazard. Mater. **285**, 398 (2015)
8. Soliman, A. A., El-Hoshoudy, A. N., Attia, A. M. Oil Gas Sci. Technol. **75**, 12 (2020)
9. L. Wu, Z. Zhao, H. Yu, M. Wang, G. Li, H. Li, J. Yan, Catal. Sci. Technol. **10**, 7481 (2020)
10. N. Malesic-Eleftheriadou, E. Evgenidou, G.Z. Kyzas, D.N. Bikiaris, D.A. Lambropoulou, Chemosphere **234**, 746 (2019)
11. A.R. Ribeiro, O.C. Nunes, M.F.R. Pereira, A.M.T. Silva, Environ. Int. **75**, 33 (2015)
12. D. Fatta-Kassinos, M.I. Vasquez, K. Kümmerer, Chemosphere **85**, 693 (2011)
13. M. Malakootian, M.A. Gharaghani, A. Dehdarirad, M. Khatami, M. Ahmadian, M.R. Heidari, H. Mahdizadeh, J. Mol. Struct. **1176**, 766 (2019)
14. Sandid, A. Marni, M. Bassyouni, Driss Nehari, Y. Elhenawy. Ener Conversat Manage **243**, 114431 (2021)
15. A.M. Chávez, O. Gimeno, A. Rey, G. Pliego, A.L. Oropesa, P.M. Álvarez, F.J. Beltrán, Chem. Eng. J. **361**, 89 (2019)
16. S.O. Ganiyu, M. Zhou, C.A. Martínez-Huitle, Appl. Catal. B Environ. **235**, 103 (2018)
17. M. Sillanpää, M.C. Ncibi, A. Matilainen, J. Environ. Manage. **208**, 56 (2018)
18. E.H. Zhou, B.H. Li, W.X. Chen, Z. Luo, J. Liu, A. Singh, A. Kumar, J.C. Jin, J. Mol. Struct. **1149**, 352 (2017)
19. Q. Li, G. Wei, Y. Yang, Z. Li, L. Zhang, L. Shao, S. Lai, Catal. Sci. Technol. **10**, 7365 (2020)
20. M.C. Ariza-Tarazona, J.F. Villarreal-Chiu, V. Barbieri, C. Siligardi, E.I. Cedillo-González, Ceram. Int. **45**, 9618 (2019)
21. F.C. Moreira, R.A.R. Boaventura, E. Brillas, V.J.P. Vilar, Appl. Catal. B Environ. **202**, 217 (2017)
22. U.I. Gaya, A.H. Abdullah, J. Photochem. Photobiol. C Photochem. Rev. **9**, 1 (2008)
23. N.N. Mahamuni, Y.G. Adewuyi, Ultrason. Sonochem. **17**, 990 (2010)
24. A. Matilainen, M. Sillanpää, Chemosphere **80**, 351 (2010)
25. J.L. Wang, L.J. Xu, Crit. Rev. Environ. Sci. Technol. **42**, 251 (2012)
26. D. Kubo, Y. Kawase, J. Clean. Prod. **203**, 685 (2018)
27. M. Cheng, G. Zeng, D. Huang, C. Lai, P. Xu, C. Zhang, Y. Liu, Chem. Eng. J. **284**, 582 (2016)
28. Y. Zhu, R. Zhu, Y. Xi, J. Zhu, G. Zhu, and H. He, Appl. Catal. B Environ. **255**, 117739 (2019).
29. I.M. Arabatzis, S. Antonaraki, T. Stergiopoulos, A. Hiskia, E. Papaconstantinou, M.C. Bernard, P. Falaras, J. Photochem. Photobiol. A Chem. **149**, 237 (2002)
30. B. Rhouta, L. Bouna, F. Maury, F. Senocq, M.C. Lafont, A. Jada, M. Amjoud, L. Daoudi, Appl. Clay Sci. **115**, 266 (2015)
31. B. Srikanth, R. Goutham, R. Badri Narayan, A. Ramprasath, K. P. Gopinath, and A. R. Sankaranarayanan, J. Environ. Manage. **200**, 60 (2017).
32. H. Veisi, J. Gholami, H. Ueda, P. Mohammadi, M. Noroozi, J. Mol. Catal. A Chem. **396**, 216 (2015)
33. S. Leong, A. Razmjou, K. Wang, K. Hapgood, X. Zhang, H. Wang, J. Memb. Sci. **472**, 167 (2014)
34. F. Li, Z. Liang, X. Zheng, W. Zhao, M. Wu, Z. Wang, Aquat. Toxicol. **158**, 1 (2015)
35. A. Elminshawy, N. Kamal Morad, A.S. Elminshawy, Y. Elhenawy. Int J Ener Res **45**(2), 2959–2979 (2021)
36. M. Sendra, I. Moreno-Garrido, M.P. Yeste, J.M. Gatica, J. Blasco, Environ. Pollut. **227**, 39 (2017)
37. M.G. Alalm, R. Djellabi, D. Meroni, C. Pirola, C.L. Bianchi, D.C. Boffito, Catalysts **11**, 1 (2021)
38. M. Samy, M. G. Ibrahim, M. Fujii, K. E. Diab, M. ElKady, and M. Gar Alalm, Chem. Eng. J. **406**, 127152 (2021).
39. K.M. Reza, A. Kurny, F. Gulshan, Appl. Water Sci. **7**, 1569 (2017)
40. Y. Shen, Q. Xu, D. Gao, H. Shi, Ozone Sci. Eng. **39**, 219 (2017)
41. M. Mishra, D.M. Chun, Appl. Catal. A Gen. **498**, 126 (2015)
42. B. Szczepanik, Appl. Clay Sci. **141**, 227 (2017)
43. J.A. Byrne, P.S.M. Dunlop, J.W.J. Hamilton, P. Fernández-Ibáñez, I. Polo-López, P.K. Sharma, A.S.M. Vennard, Molecules **20**, 5574 (2015)
44. Q. Cheng, C. Wang, K. Doudrick, C.K. Chan, Appl. Catal. B Environ. **176–177**, 740 (2015)
45. S.G. Kumar, K.S.R.K. Rao, Appl. Surf. Sci. **391**, 124 (2017)
46. S.V. Mohite, V.V. Ganbavle, V.V. Patil, K.Y. Rajpure, Mater. Chem. Phys. **183**, 439 (2016)
47. M. Arshad, M. Abbas, S. Ehtisham-ul-Haque, M.A. Farrukh, A. Ali, H. Rizvi, G.A. Soomro, A. Ghaffar, M. Yameen, M. Iqbal, J. Mol. Struct. **1180**, 244 (2019)
48. F. Liang, M. Lu, Y. Zhang, Q. Shi, and F. Shi, J. Mol. Struct. 129636 (2020).
49. T. Zhou, X. Huang, H. Zhang, H. Yang, K. Ma, P. Zhang, G. Zhang, Catal. Sci. Technol. **10**, 7661 (2020)
50. T. Raguram, K.S. Rajni, Appl. Phys. A Mater. Sci. Process. **125**, 1 (2019)

51. H. Yu, P. Xiao, P. Wang, J. Yu, Appl. Catal. B Environ. **193**, 217 (2016)
52. Y. Markushyna, C. Teutloff, B. Kurpil, D. Cruz, I. Lauermann, Y. Zhao, M. Antonietti, and A. Savateev, Appl. Catal. B Environ. 211 (2019).
53. W.J. Ong, L.K. Putri, L.L. Tan, S.P. Chai, S.T. Yong, Appl. Catal. B Environ. **180**, 530 (2016)
54. E. Sathiyaraj and S. Thirumaran, Chem. Phys. Lett. **739**, 136972 (2020).
55. M. Anjum, R. Kumar, M.A. Barakat, J. Taiwan Inst. Chem. Eng. **77**, 227 (2017)
56. C. Karthikeyan, P. Arunachalam, K. Ramachandran, A. M. Al-Mayouf, and S. Karuppuchamy, J. Alloys Compd. **828**, 154281 (2020).
57. M. Junaid, M. Imran, M. Ikram, M. Naz, M. Aqeel, H. Afzal, H. Majeed, S. Ali, Appl. Nanosci. **9**, 1593 (2019)
58. X. Li, J. Xie, C. Jiang, J. Yu, P. Zhang, Front. Environ. Sci. Eng. **12**, 1 (2018)
59. H. Zabihi-Mobarakeh, A. Nezamzadeh-Ejhieh, J. Ind. Eng. Chem. **26**, 315 (2015)
60. P. Ribao, J. Corredor, M. J. Rivero, and I. Ortiz, J. Hazard. Mater. 45 (2019).
61. A. Nezamzadeh-Ejhieh, N. Moazzeni, J. Ind. Eng. Chem. **19**, 1433 (2013)
62. S. Chowdhury, R. Balasubramanian, Appl. Catal. B Environ. **160–161**, 307 (2014)
63. J. Bedia, V. Muelas-Ramos, M. Peñas-Garzón, A. Gómez-Avilés, J. J. Rodríguez, and C. Belver, Catalysts **9**, (2019).
64. S. N. Ahmed and W. Haider, Nanotechnology **29**, (2018).
65. Z. Zhu, Y. Chen, Y. Gu, F. Wu, W. Lu, T. Xu, W. Chen, Water Res. **93**, 296 (2016)
66. Y.L. Pang, A.Z. Abdullah, S. Bhatia, DES **277**, 1 (2011)
67. B. Boruah, R. Gupta, J.M. Modak, G. Madras, J. Photochem. Photobiol. A Chem. **373**, 105 (2019)
68. S. Rahim Pouran, A. A. Abdul Raman, and W. M. A. Wan Daud, J. Clean. Prod. **64**, 24 (2014).
69. F. Han, V.S.R. Kambala, M. Srinivasan, D. Rajarathnam, R. Naidu, Appl. Catal. A Gen. **359**, 25 (2009)
70. A.M. Botero-Coy, D. Martínez-Pachón, C. Boix, R.J. Rincón, N. Castillo, L.P. Arias-Marín, L. Manrique-Losada, R. Torres-Palma, A. Moncayo-Lasso, F. Hernández, Sci. Total Environ. **642**, 842 (2018)
71. D. Kanakaraju, B.D. Glass, M. Oelgemöller, J. Environ. Manage. **219**, 189 (2018)
72. M. Ibáñez, V. Borova, C. Boix, R. Aalizadeh, R. Bade, N.S. Thomaidis, F. Hernández, J. Hazard. Mater. **323**, 26 (2017)
73. C. Nebot, R. Falcon, K.G. Boyd, S.W. Gibb, Environ. Sci. Pollut. Res. **22**, 10559 (2015)
74. A. Shraim, A. Diab, A. Alsuhaimi, E. Niazy, M. Metwally, M. Amad, S. Sioud, A. Dawoud, Arab. J. Chem. **10**, S719 (2017)
75. M. Oliveira Miranda, W. Eulálio Cabral Cavalcanti, F. Ivan Da Silva, E. Rigoti, E. Rodríguez-Castellón, S. B. C. Pergher, and T. Pinheiro Braga, Catal. Sci. Technol. **10**, 7681 (2020).
76. V. de Jesus Gaffney, C. M. M. Almeida, A. Rodrigues, E. Ferreira, M. J. Benoliel, and V. V. Cardoso, Water Res. **72**, 199 (2015).
77. S. González-Alonso, L.M. Merino, S. Esteban, M. López de Alda, D. Barceló, J.J. Durán, J. López-Martínez, J. Aceña, S. Pérez, N. Mastroianni, A. Silva, M. Catalá, Y. Valcárcel, Environ. Pollut. **229**, 241 (2017)
78. S. Matongo, G. Birungi, B. Moodley, P. Ndungu, Chemosphere **134**, 133 (2015)
79. J. Sun, Q. Luo, D. Wang, Z. Wang, Ecotoxicol. Environ. Saf. **117**, 132 (2015)
80. P. Paíga, C. Delerue-Matos, Sci. Total Environ. **569–570**, 16 (2016)
81. M. Zemann, M. Majewsky, L. Wolf, Chemosphere **154**, 463 (2016)
82. M. Caban, E. Lis, J. Kumirska, P. Stepnowski, Sci. Total Environ. **538**, 402 (2015)
83. J. Wang, S. Wang, J. Environ. Manage. **182**, 620 (2016)
84. S. Naraginti, Y. Li, Y. Wu, C. Zhang, A.R. Upreti, RSC Adv. **6**, 87246 (2016)
85. J. Rivera-Utrilla, M. Sánchez-Polo, M.Á. Ferro-García, G. Prados-Joya, R. Ocampo-Pérez, Chemosphere **93**, 1268 (2013)
86. A. Ziylan, N.H. Ince, J. Hazard. Mater. **187**, 24 (2011)
87. S.K. Mondal, A.K. Saha, A. Sinha, J. Clean. Prod. **171**, 1203 (2018)
88. T.G. Bean, B.A. Rattner, R.S. Lazarus, D.D. Day, S.R. Burket, B.W. Brooks, S.P. Haddad, W.W. Bowerman, Environ. Pollut. **232**, 533 (2018)
89. K. G. Pavithra, S. K. P., V. Jaikumar, and S. R. P., J. Ind. Eng. Chem. **75**, 1 (2019).
90. V. Homem, L. Santos, J. Environ. Manage. **92**, 2304 (2011)
91. P.-S. Konstas, C. Kosma, I. Konstantinou, T. Albanis, Water **11**, 2165 (2019)
92. A. Aghaeinejad-Meybodi, A. Ebadi, S. Shafiei, A.R. Khataee, M. Rostampour, J. Taiwan Inst. Chem. Eng. **48**, 40 (2015)
93. N. Taoufik, W. Boumya, F. Z. Janani, A. Elhalil, F. Z. Mahjoubi, and N. barka, J. Environ. Chem. Eng. **8**, 104251 (2020).
94. K. Fouad, M. Bassyouni, M.G. Alalm, M.Y. Saleh, J. Environ. Treat. Tech. **9**, 499 (2021)
95. D. Awfa, M. Ateia, M. Fujii, M.S. Johnson, C. Yoshimura, Water Res. **142**, 26 (2018)
96. E.O. Reis, A.F.S. Foureaux, J.S. Rodrigues, V.R. Moreira, Y.A.R. Lebron, L.V.S. Santos, M.C.S. Amaral, L.C. Lange, Environ. Pollut. **250**, 773 (2019)
97. A.E. Rodríguez-Mata, L.E. Amabilis-Sosa, A. Roé-Sosa, J.M. Barrera-Andrade, J.G. Rangel-Peraza, M.G. Salinas-Juárez, Korean J. Chem. Eng. **36**, 423 (2019)
98. N. Bustos, A. Cruz-Alcalde, A. Iriel, A. Fernández Cirelli, and C. Sans, Sci. Total Environ. **649**, 592 (2019).
99. M. Abdennouri, M. Baâlala, A. Galadi, M. El Makhfouk, M. Bensitel, K. Nohair, M. Sadiq, A. Boussaoud, N. Barka, Arab. J. Chem. **9**, S313 (2016)
100. M. Kanwal, S.R. Tariq, G.A. Chotana, Environ. Sci. Pollut. Res. **25**, 27307 (2018)
101. M.J. Climent, E. Herrero-Hernández, M.J. Sánchez-Martín, M.S. Rodríguez-Cruz, P. Pedreros, R. Urrutia, Environ. Pollut. **251**, 90 (2019)
102. E. Carazo-Rojas, G. Pérez-Rojas, M. Pérez-Villanueva, C. Chinchilla-Soto, J.S. Chin-Pampillo, P. Aguilar-Mora, M. Alpízar-Marín, M. Masís-Mora, C.E. Rodríguez-Rodríguez, Z. Vryzas, Environ. Pollut. **241**, 800 (2018)
103. M. Bilal, H. M. N. Iqbal, and D. Barceló, Sci. Total Environ. **695**, (2019).
104. J. Singh, S. Sharma, Aanchal, and S. Basu, J. Photochem. Photobiol. A Chem. **376**, 32 (2019).
105. W. He, J.M. Fontmorin, I. Soutrel, D. Floner, F. Fourcade, A. Amrane, F. Geneste, Mol. Catal. **432**, 8 (2017)
106. S. Sajjadi, A. Khataee, N. Bagheri, M. Kobya, A. Şenocak, E. Demirbas, A.G. Karaoğlu, J. Ind. Eng. Chem. **77**, 280 (2019)
107. M.L. Yola, T. Eren, N. Atar, Chem. Eng. J. **250**, 288 (2014)
108. R. Jayaraj, P. Megha, P. Sreedev, Interdiscip. Toxicol. **9**, 90 (2016)
109. M. Jackson, C. Eadsforth, D. Schowanek, T. Delfosse, A. Riddle, N. Budgen, Environ. Toxicol. Chem. **35**, 1077 (2016)
110. S. Krishnan, K. Chandran, C.M. Sinnathambi, Int. J. Appl. Chem. **12**, 727 (2016)
111. K. Ikehata, M.G. El-Din, Ozone Sci. Eng. **26**, 327 (2004)
112. B. Mondal, A. Adak, P. Datta, J. Photochem. Photobiol. A Chem. **375**, 237 (2019)

113. F. Ríos, M. Olak-Kucharczyk, M. Gmurek, S. Ledakowicz, Arch. Environ. Prot. **43**, 20 (2017)
114. Z. Noorimotlagh, I. Kazeminezhad, N. Jaafarzadeh, and M. Ahmadi, Catal. Today 0 (2019).
115. S. Li, G. Zhang, W. Zhang, H. Zheng, W. Zhu, N. Sun, Y. Zheng, P. Wang, Chem. Eng. J. **326**, 756 (2017)
116. B. Gomez-Ruiz, P. Ribao, N. Diban, M.J. Rivero, I. Ortiz, A. Urtiaga, J. Hazard. Mater. **344**, 950 (2018)
117. E. Brillas, C.A. Martínez-Huitle, Appl. Catal. B Environ. **166–167**, 603 (2015)
118. S. Pourmasoud, A. Sobhani-Nasab, M. Behpour, M. Rahimi-Nasrabadi, F. Ahmadi, J. Mol. Struct. **1157**, 607 (2018)
119. M. Jafari, M.R. Rahimi, M. Ghaedi, K. Dashtian, Chem. Eng. Res. Des. **125**, 408 (2017)
120. M.H. Abdel-Aziz, M. Bassyouni, M.S. Zoromba, A.A. Alshehri, Ind. Eng. Chem. Res. **58**, 1004 (2019)
121. R. Saravanan, S. Karthikeyan, V.K. Gupta, G. Sekaran, V. Narayanan, A. Stephen, Mater. Sci. Eng. C **33**, 91 (2013)
122. A. Asghar, A.A.A. Raman, W.M.A.W. Daud, J. Clean. Prod. **87**, 826 (2015)
123. F. R. Abe, A. M. V. M. Soares, D. P. d. Oliveira, and C. Gravato, Environ. Pollut. **235**, 255 (2018).
124. M. Samadi, M. Zirak, A. Naseri, M. Kheirabadi, M. Ebrahimi, A.Z. Moshfegh, *Design and Tailoring of One-Dimensional ZnO Nanomaterials for Photocatalytic Degradation of Organic Dyes: A Review* (Springer, Netherlands, 2019)
125. M.A. Mahadik, S.S. Shinde, V.S. Mohite, S.S. Kumbhar, A.V. Moholkar, K.Y. Rajpure, V. Ganesan, J. Nayak, S.R. Barman, C.H. Bhosale, J. Photochem. Photobiol. B Biol. **133**, 90 (2014)
126. T. Karnan, S.A.S. Selvakumar, J. Mol. Struct. **1125**, 358 (2016)
127. A. Omidvar, B. Jaleh, M. Nasrollahzadeh, H.R. Dasmeh, Chem. Eng. Res. Des. **121**, 339 (2017)
128. H. Anwer, A. Mahmood, J. Lee, K.-H. Kim, J.-W. Park, A.C.K. Yip, Nano Res. **12**, 955 (2019)
129. N. Muhd Julkapli, S. Bagheri, and S. Bee Abd Hamid, Sci. World J. **2014**, (2014).
130. D. Ayodhya, G. Veerabhadram, Mater. Today. Energy **9**, 83 (2018)
131. S.V.P. Vattikuti, Y.J. Baik, C. Byon, Mater. Express **6**, 161 (2016)
132. H. Jafari, S. Afshar, O. Zabihi, M. Naebe, Res. Chem. Intermed. **42**, 2963 (2016)
133. L. Khaledi Maki, A. Maleki, R. Rezaee, H. Daraei, and K. Yetilmezsoy, Environ. Technol. Innov. **15**, 100411 (2019).
134. A.G. Akerdi, S.H. Bahrami, M. Arami, E. Pajootan, Chemosphere **159**, 293 (2016)
135. A. Dąbrowski, P. Podkościelny, Z. Hubicki, and M. Barczak, Chemosphere **58**, 1049 (2005).
136. S. Ahmed, M.G. Rasul, W.N. Martens, R. Brown, M.A. Hashib, Desalination **261**, 3 (2010)
137. Z. Guo, R. Ma, G. Li, Chem. Eng. J. **119**, 55 (2006)
138. R. Xiao, L. Gao, Z. Wei, R. Spinney, S. Luo, D. Wang, D.D. Dionysiou, C.J. Tang, W. Yang, Environ. Pollut. **231**, 1446 (2017)
139. C.M. Teh, A.R. Mohamed, J. Alloys Compd. **509**, 1648 (2011)
140. I. Ignat, I. Volf, V.I. Popa, Food Chem. **126**, 1821 (2011)
141. S.K. Pardeshi, A.B. Patil, Sol. Energy **82**, 700 (2008)
142. N.A. Sabri, M.A. Nawi, W.I. Nawawi, Opt. Mater. (Amst). **48**, 258 (2015)
143. S. Sarkar, S. Chakraborty, C. Bhattacharjee, Ecotoxicol. Environ. Saf. **121**, 263 (2015)
144. M. R. Maurya, A. Kumar, and J. Costa Pessoa, Coord. Chem. Rev. **255**, 2315 (2011).
145. S. Teixeira, P.M. Martins, S. Lanceros-Méndez, K. Kühn, G. Cuniberti, Appl. Surf. Sci. **384**, 497 (2016)
146. S. Ramasundaram, M.G. Seid, J.W. Choe, E.J. Kim, Y.C. Chung, K. Cho, C. Lee, S.W. Hong, Chem. Eng. J. **306**, 344 (2016)
147. R. Oblak, M. Kete, U.L. Štangar, M. Tasbihi, J. Water Process Eng. **23**, 142 (2018)
148. M. Behpour, P. Shirazi, M. Rahbar, React. Kinet. Mech. Catal. **127**, 1073 (2019)
149. H. Fang, J. Zheng, X. Luo, J. Du, A. Roldan, S. Leoni, Y. Yuan, Appl. Catal. A Gen. **529**, 20 (2017)
150. J. Zdarta, A. S. Meyer, T. Jesionowski, and M. Pinelo, Catalysts **8**, (2018).
151. A.Y. Shan, T.I.M. Ghazi, S.A. Rashid, Appl. Catal. A Gen. **389**, 1 (2010)
152. G.J. Owens, R.K. Singh, F. Foroutan, M. Alqaysi, C.-M. Han, C. Mahapatra, H.-W. Kim, J.C. Knowles, Prog. Mater. Sci. **77**, 1 (2016)
153. A. C. Jones and M. L. Hitchman, *Overview of Chemical Vapour Deposition* (2009).
154. M. Naebe, K. Shirvanimoghaddam, Appl. Mater. Today **5**, 223 (2016)
155. P. Marchand, I.A. Hassan, I.P. Parkin, C.J. Carmalt, Dalt. Trans. **42**, 9406 (2013)
156. M.S. Ata, Y. Liu, I. Zhitomirsky, RSC Adv. **4**, 22716 (2014)
157. N. Alonizan, S. Rabaoui, K. Omri, R. Qindeel, Appl. Phys. A Mater. Sci. Process. **124**, 1 (2018)
158. L. Besra, M. Liu, Prog. Mater. Sci. **52**, 1 (2007)
159. S. Hu, W. Li, H. Finklea, and X. Liu, Adv. Colloid Interface Sci. **276**, 102102 (2020).
160. M. Ammam, RSC Adv. **2**, 7633 (2012)
161. I. Corni, M.P. Ryan, A.R. Boccaccini, J. Eur. Ceram. Soc. **28**, 1353 (2008)
162. I. A. Neacşu, A. I. Nicoară, O. R. Vasile, and B. Ş. Vasile, Nanobiomaterials Hard Tissue Eng. Appl. Nanobiomaterials 271 (2016).
163. M. Harju and T. Ma, **249**, 115 (2005).
164. K. Sarakinos, J. Alami, S. Konstantinidis, Surf. Coatings Technol. **204**, 1661 (2010)
165. A. Anders, Surf. Coatings Technol. **204**, 2864 (2010)
166. M. Mokhtary, J. Iran. Chem. Soc. **13**, 1827 (2016)
167. N.M. Mahmoodi, M. Arami, J. Zhang, J. Alloys Compd. **509**, 4754 (2011)
168. N. Miranda-García, S. Suárez, B. Sánchez, J.M. Coronado, S. Malato, M.I. Maldonado, Appl. Catal. B Environ. **103**, 294 (2011)
169. G. Mascolo, R. Comparelli, M.L. Curri, G. Lovecchio, A. Lopez, A. Agostiano, J. Hazard. Mater. **142**, 130 (2007)
170. S. Singh, H. Mahalingam, P.K. Singh, Appl. Catal. A Gen. **462–463**, 178 (2013)
171. M. Bideau, B. Claudel, C. Dubien, L. Faure, H. Kazouan, J. Photochem. Photobiol. A Chem. **91**, 137 (1995)
172. K. Pirkanniemi, M. Sillanpää, Chemosphere **48**, 1047 (2002)
173. U. Černigoj, U.L. Štangar, P. Trebše, J. Photochem. Photobiol. A Chem. **188**, 169 (2007)
174. B.M. Weckhuysen, J. Yu, Chem. Soc. Rev. **44**, 7022 (2015)
175. L. Xu, Y. Yuan, Q. Han, L. Dong, L. Chen, X. Zhang, and L. Xu, Catal. Sci. Technol. 7904 (2020).
176. Z. Li, L. Wang, J. Meng, X. Liu, J. Xu, F. Wang, P. Brookes, J. Hazard. Mater. **344**, 1 (2018)
177. M. Huang, C. Xu, Z. Wu, Y. Huang, J. Lin, J. Wu, Dye. Pigment. **77**, 327 (2008)
178. J. Čejka, R.E. Morris, D.P. Serrano, Catal. Sci. Technol. **6**, 2465 (2016)
179. Z. Li, X. Jiang, G. Xiong, B. Nie, C. Liu, N. He, and J. Liu, Catal. Sci. Technol. (2020).
180. S. Gomez, C.L. Marchena, M.S. Renzini, L. Pizzio, L. Pierella, Appl. Catal. B Environ. **162**, 167 (2015)
181. M. Danish, X. Gu, S. Lu, U. Farooq, W.Q. Zaman, X. Fu, Z. Miao, M.L. Brusseau, A. Ahmad, M. Naqvi, Appl. Catal. A Gen. **531**, 177 (2017)

182. C. Leal Marchena, L. Lerici, S. Renzini, L. Pierella, and L. Pizzio, Appl. Catal. B Environ. **188**, 23 (2016).
183. G. Liao, W. He, and Y. He, Catalysts **9**, (2019).
184. N. Ajoudanian, A. Nezamzadeh-Ejhieh, Mater. Sci. Semicond. Process. **36**, 162 (2015)
185. R.M. Cámara, E. Crespo, R. Portela, S. Suárez, L. Bautista, F. Gutiérrez-Martín, B. Sánchez, Catal. Today **230**, 145 (2014)
186. M. Sökmen, I. Tatlidil, C. Breen, F. Clegg, C.K. Buruk, T. Sivlim, Ş Akkan, J. Hazard. Mater. **187**, 199 (2011)
187. M. Cantarella, R. Sanz, M.A. Buccheri, F. Ruffino, G. Rappazzo, S. Scalese, G. Impellizzeri, L. Romano, V. Privitera, J. Photochem. Photobiol. A Chem. **321**, 1 (2016)
188. Z.A.M. Hir, P. Moradihamedani, A.H. Abdullah, M.A. Mohamed, Mater. Sci. Semicond. Process. **57**, 157 (2017)
189. N. Jallouli, K. Elghniji, H. Trabelsi, M. Ksibi, Arab. J. Chem. **10**, S3640 (2017)
190. L. Aoudjit, P.M. Martins, F. Madjene, D.Y. Petrovykh, S. Lanceros-Mendez, J. Hazard. Mater. **344**, 408 (2018)
191. D.R. Eddy, F.N. Puri, A.R. Noviyanti, Procedia Chem. **17**, 55 (2015)
192. Y. He, N.B. Sutton, H.H.H. Rijnaarts, A.A.M. Langenhoff, Appl. Catal. B Environ. **182**, 132 (2016)
193. T. Ben-Moshe, I. Dror, B. Berkowitz, Water. Air. Soil Pollut. **223**, 3105 (2012)
194. U. Patil, S.C. Lee, S. Kulkarni, J.S. Sohn, M.S. Nam, S. Han, S.C. Jun, Nanoscale **7**, 6999 (2015)
195. K. He, G. Chen, G. Zeng, A. Chen, Z. Huang, J. Shi, T. Huang, M. Peng, L. Hu, Appl. Catal. B Environ. **228**, 19 (2018)
196. M. Nawaz, W. Miran, J. Jang, D.S. Lee, Appl. Catal. B Environ. **203**, 85 (2017)
197. V.S. Kosera, T.M. Cruz, E.S. Chaves, E.R.L. Tiburtius, J. Photochem. Photobiol. A Chem. **344**, 184 (2017)
198. A. Shet, S.K. Vidya, Sol. Energy **127**, 67 (2016)
199. M. Rani, U. Shanker, A.K. Chaurasia, J. Environ. Chem. Eng. **5**, 2730 (2017)
200. J. Ye, X. Li, J. Hong, J. Chen, Q. Fan, Mater. Sci. Semicond. Process. **39**, 17 (2015)
201. M. N. I. Amir, N. Muhd Julkapli, and S. B. A. Hamid, Mater. Technol. **32**, 256 (2017).
202. R. Darvishi Cheshmeh Soltani, A. Rezaee, M. Safari, A. R. Khataee, and B. Karimi, Desalin. Water Treat. **53**, 1613 (2015).
203. A. Maleki, M. Safari, R. Rezaee, R. D. Cheshmeh Soltani, B. Shahmoradi, and Y. Zandsalimi, Sep. Sci. Technol. **51**, 2484 (2016).
204. M. Shokri, G. Isapour, M.A. Behnajady, S. Dorosti, Desalin. Water Treat. **57**, 12874 (2016)
205. M. Gar Alalm, M. Samy, S. Ookawara, and T. Ohno, J. Water Process Eng. **26**, 329 (2018).
206. M.P. Seabra, E. Rego, A. Ribeiro, J.A. Labrincha, Chem. Eng. J. **171**, 175 (2011)
207. M. Mirzaei, B. Dabir, M. Dadvar, M. Jafarikojour, Ind. Eng. Chem. Res. **56**, 1739 (2017)
208. S. Murgolo, V. Yargeau, R. Gerbasi, F. Visentin, N. El Habra, G. Ricco, I. Lacchetti, M. Carere, M.L. Curri, G. Mascolo, Chem. Eng. J. **318**, 103 (2017)
209. K. Fouad, M. Gar Alalm, M. Bassyouni, and M. Y. Saleh, Chemosphere **257**, 127270 (2020).
210. A. Verma, A.P. Toor, N.T. Prakash, P. Bansal, V.K. Sangal, New J. Chem. **41**, 6296 (2017)
211. A.M. Khaksar, S. Nazif, A. Taebi, E. Shahghasemi, J. Photochem. Photobiol. A Chem. **348**, 161 (2017)
212. A. Manassero, M. L. Satuf, and O. M. Alfano, Chem. Eng. J. (2017).
213. X. Gong, H. Wang, C. Yang, Q. Li, X. Chen, and J. Hu, Futur. Cities Environ. 1 (2015).
214. S. Zhong, C. Lv, S. Zou, F. Zhang, S. Zhang, J. Mater. Sci. Mater. Electron. **29**, 2447 (2018)
215. T. Claes, A. Dilissen, M.E. Leblebici, T. Van Gerven, Chem. Eng. J. **361**, 725 (2019)
216. Y. Zhang, G. Shan, F. Dong, C. Wang, L. Zhu, J. Environ. Sci. **80**, 277 (2019)
217. H. O'Neal Tugaoen, S. Garcia-Segura, K. Hristovski, and P. Westerhoff, Sci. Total Environ. **613–614**, 1331 (2018).
218. L. Lin, H. Wang, P. Xu, Chem. Eng. J. **310**, 389 (2017)
219. M. Karaca, M. Kiranşan, S. Karaca, A. Khataee, A. Karimi, Ultrason. Sonochem. **31**, 250 (2016)
220. H. Zhang, P. Zhang, Y. Ji, J. Tian, Z. Du, Chem. Eng. J. **262**, 1108 (2015)
221. M. Kovacic, S. Salaeh, H. Kusic, A. Suligoj, M. Kete, M. Fanetti, U.L. Stangar, D.D. Dionysiou, A.L. Bozic, Environ. Sci. Pollut. Res. **23**, 17982 (2016)
222. A.J. Expósito, D.A. Patterson, W.S.W. Mansor, J.M. Monteagudo, E. Emanuelsson, I. Sanmartín, A. Durán, J. Environ. Manage. **187**, 504 (2017)
223. M. Ahmadi, H. Ramezani Motlagh, N. Jaafarzadeh, A. Mostoufi, R. Saeedi, G. Barzegar, and S. Jorfi, J. Environ. Manage. **186**, 55 (2017).
224. L. Li, X. Zheng, Y. Chi, Y. Wang, X. Sun, Q. Yue, and B. Gao, J. Hazard. Mater. **383**, 121211 (2020).
225. M. Malakootian, A. Nasiri, and M. Amiri Gharaghani, Chem. Eng. Commun. **207**, 56 (2020).
226. M. Malakootian, H. Mahdizadeh, A. Dehdarirad, and M. Amiri Gharghani, J. Dispers. Sci. Technol. **40**, 846 (2019).
227. M. Samy, M. G. Ibrahim, M. Gar Alalm, M. Fujii, S. Ookawara, and T. Ohno, J. Water Process Eng. **33**, 3 (2020).
228. H. Karimnezhad, A. H. Navarchian, T. Tavakoli Gheinani, and S. Zinadini, Chem. Eng. Res. Des. **153**, 187 (2020).
229. A. Khataee and M. Kıran, **0**, 1 (2017).
230. P. Bansal, A. Verma, J. Photochem. Photobiol. A Chem. **342**, 131 (2017)
231. E. A. De Campos and C. R. Pazini, Biochem. Pharmacol. (2018).
232. V. Pí, **305**, 19 (2015).
233. M.J. Arlos, R. Liang, M.M. Hatat-fraile, L.M. Bragg, N.Y. Zhou, M.R. Servos, S.A. Andrews, J. Hazard. Mater. **318**, 541 (2016)
234. A. Sraw, T. Kaur, Y. Pandey, A. Sobti, R. K. Wanchoo, and A. P. Toor, Biochem. Pharmacol. (2018).
235. T. Ahmadifard, R. Heydari, M.J. Tarrahi, G.S. Khorramabadi, Int. J. Chem. React. Eng. **17**, 1 (2019)
236. A. Maleki, F. Moradi, B. Shahmoradi, R. Rezaee, and S. M. Lee, J. Mol. Liq. **297**, 111918 (2020).
237. K. Sivagami, R. Ravi Krishna, and T. Swaminathan, Desalin. Water Treat. **57**, 28822 (2016).
238. I.C. M'Bra, P. García-Muñoz, P. Drogui, N. Keller, A. Trokourey, D. Robert, J. Photochem. Photobiol. A Chem. **368**, 1 (2019)
239. T. Kaur, A. Sraw, R.K. Wanchoo, A.P. Toor, Sol. Energy **162**, 45 (2018)
240. P. Mohammadi, H. Sheibani, Polyhedron **170**, 132 (2019)
241. A. Rahmani, H. Rahimzadeh, S. Beirami, Desalin. Water Treat. **144**, 224 (2019)
242. I. Othman, M. Abu Haija, I. Ismail, J. H. Zain, and F. Banat, Mater. Chem. Phys. **238**, 121931 (2019).
243. F. Soori, A. Nezamzadeh-Ejhieh, J. Mol. Liq. **255**, 250 (2018)
244. H. Lee, P. Kannan, A. Al Shoaibi, and C. Srinivasakannan, J. Water Process Eng. **31**, 100869 (2019).
245. Y. Shao, J. Ruan, X. Li, Y. Li, H. Chen, Process Saf. Environ. Prot. **136**, 288 (2020)

Authors and Affiliations

Kareem Fouad[1,2] · Mohamed Bassyouni[3,4] · Mohamed Gar Alalm[5,6] · Mamdouh Y. Saleh[1]

1 Department of Civil Engineering, Faculty of Engineering, Port Said University, Port Said 42526, Egypt

2 Department of Civil Engineering, Higher Institute of Engineering and Technology, New Damietta 34517, Egypt

3 Department of Chemical Engineering, Faculty of Engineering, Port Said University, Port Said 42526, Egypt

4 Materials Science Program, University of Science and Technology, Zewail City of Science and Technology, October Gardens, 6th of October, Giza 12578, Egypt

5 Department of Chemical Engineering, Polytechnique Montréal, Montréal, Succ. CV C.P. 6079H3C 3A7, Canada

6 Department of Public Works Engineering, Faculty of Engineering, Mansoura University, Mansoura 35516, Egypt